AN INVESTIGATION ON DYNAMIC CONTACT PARAMETERS IN MACHINING CENTER SPINDLE – TOOL ASSEMBLIES

A THESIS SUBMITTED TO
THE GRADUATE SCHOOL OF NATURAL AND APPLIED SCIENCES
OF
MIDDLE EAST TECHNICAL UNIVERSITY

BY

ORKUN ÖZŞAHİN

IN PARTIAL FULFILMENT OF THE REQUIREMENTS
FOR
THE DEGREE OF MASTER OF SCIENCE
IN
MECHANICAL ENGINEERING

AUGUST 2008

Approval of the Thesis

An Investigation on Dynamic Contact Parameters in Machining Center Spindle – Tool Assemblies

submitted by **ORKUN ÖZŞAHİN** in partial fulfillment of requirement for the degree of **Master of Science in Mechanical Engineering Department, Middle East Technical University** by,

Prof. Dr. Canan ÖZGEN _____
Dean, Graduate School of **Natural and Applied Sciences**

Prof. Dr. S. Kemal İDER _____
Head of the Department, **Mechanical Engineering**

Prof. Dr. H. Nevzat ÖZGÜVEN _____
Supervisor, **Mechanical Engineering Dept., METU**

Assoc.Prof. Dr. Erhan BUDAK _____
Co-Supervisor, **Faculty of Engineering and Natural Sciences, SU**

Examining Committee Members

Prof. Dr. Samim Ünlüsoy _____
Mechanical Engineering Dept., METU

Prof. Dr. H. Nevzat ÖZGÜVEN _____
Mechanical Engineering Dept., METU

Assoc.Prof. Dr. Erhan BUDAK _____
Faculty of Engineering and Natural Sciences, SU

Asst. Prof.Dr Melin ŞAHİN _____
Aerospace Engineering Dept., METU

Asst.Prof.Dr. Gökhan ÖZGEN _____
Mechanical Engineering Dept., METU

Date: _____

I hereby declare that all information in this document has been obtained and presented in accordance with academic rules and ethical conduct. I also declare that, as required by these rules and conduct, I have fully cited and referenced all material and results that are not original to this work.

Name, Last name: Orkun ÖZŞAHİN

Signature:

ABSTRACT

An Investigation on Dynamic Contact Parameters in Machining Center Spindle – Tool Assemblies

Özşahin, Orkun

M.Sc., Department of Mechanical Engineering

Supervisor: Prof. Dr. H. Nevzat Özgüven

Co-Supervisor: Assoc. Prof. Dr. Erhan Budak

August 2008, 85pages

In machining centers, with the increasing trends in high precision machining, chatter has become an important problem which results in poor surface finish and low material removal rate. Chatter can be avoided with stability diagrams which provide the stable regions in the machining process for the depth of cut and spindle speed combinations. In order to obtain stability diagrams, tool point frequency response function (FRF) of the system should be obtained. Throughout this study, contact parameters which are the most critical part of the analytical modeling of spindle-holder-tool assembly in order to obtain tool point FRF, are examined. For the accurate identification of the contact parameters, a recently suggested closed form approach based on measured FRFs is improved and applied to real structures by solving several application problems.

In addition to the identification of contact parameters from experimental results, in order to eliminate the dependency on experiments, artificial neural networks are used to predict contact parameters for cases for which no experiments were carried out. By using trained neural network, contact parameters are predicted for the first seen combination of tool gauge length and diameter with a high accuracy. Such an application will have an important contribution to the machining stability studies since elimination of dependency on experiments will make it possible to predict stability diagrams for different combinations of spindle, holder and tool without performing any experiments.

Additionally, since accurate identification of contact parameters, thus tool point FRFs and stability diagrams are highly dependent on accuracy of the performed experiments, possible errors due the mass of the accelerometers are also investigated. In order to compensate the mass effect of the accelerometers, a structural modification with matrix inversion method is applied to the accelerometer based results.

Keywords: Chatter Stability, Contact dynamics, Contact Parameters Identification, Accelerometer Mass Effect and Neural Networks.

ÖZ

İŞLEME MERKEZLERİNDE DİNAMİK BAĞLANTI PARAMETRELERİNİN İNCELENMESİ

Özşahin, Orkun

Yüksek Lisans, Makine Mühendisliği Bölümü

Tez Yöneticisi: Prof. Dr. H. Nevzat Özgüven

Ortak Tez Yöneticisi: Doç. Dr. Erhan Budak

Ağustos 2008, 85 sayfa

İşleme merkezlerinde, yüksek hassasiyette kesme işlemlerinin artmasıyla birlikte, düşük yüzey kalitesine ve talaş kaldırma oranın azalmasına neden olan tırlama önemli bir sorun haline gelmiştir. Tırlama belirli kesme hızı ve kesme derinliği için kararlı bölgelerin elde edilmesini sağlayan kararlılık diyagramlarının kullanılması ile önlenebilir. Kararlılık diyagramlarının elde edilebilmesi için sistemin takım ucu frekans tepki fonksiyonun (FTF) belirlenmesi gerekmektedir. Bu çalışmada, takım ucu FTF'sini analitik olarak elde edilmesinde oldukça kritik bir öneme sahip olan bağlantı parametreleri incelenmiştir. Bağlantı parametrelerinin doğru bir şekilde belirlenebilmesi amacıyla, deney sonuçlarının

kullanımına dayalı yeni önerilmiş bir yöntem geliştirilmiş ve uygulamadaki çeşitli sorunlar çözülerek gerçek sistemlere uygulanmıştır.

Bağlantı parametrelerinin deney sonuçlarından belirlenmesine ek olarak, deneylere olan bağımlılığı ortadan kaldırmak ve deney yapılmayan durumlar için de bağlantı parametrelerini öngörebilmek amacıyla yapay sinir ağları uygulaması kullanılmıştır. Eğitilmiş yapay sinir ağları kullanılarak, ilk defa karşılaşılan takım uzunluğu ve takım çapı kombinasyonları için bağlantı parametreleri oldukça hasas olarak belirlenmiştir. Böylesi bir uygulama, farklı şaft, takım tutucu ve takım kombinasyonu için deney yapmadan kararlılık diyagramlarının elde edilebilmesini sağlaması açısından, kararlılık diyagramları ile ilgili çalışmalara önemli bir katkı sağlayacaktır.

Ayrıca, bağlantı parametrelerinin ve dolayısı ile takım ucu FTF'sinin ve karalılık diyagramlarının doğru bir şekilde belirlenmesi, deneylerin doğruluğuna bağlı olması nedeniyle, ivme ölçer kütle etkisinin deney sonuçları üzerine etkisi incelenmiştir. İvme ölçer kütle etkisini telafi etmek amacıyla, matris tersi yapısal değişiklik metodu ivmeölçer ile elde edilen sonuçlara uygulanmıştır.

Anahtar Kelimeler: Tırlama Kararlılığı, Bağlantı Dinamiği, Bağlantı Parametrelerinin Belirlenmesi, İvme Ölçer Kütle Etkisi, Yapay Sinir Ağları

To my Family

Acknowledgement

The author expresses sincere appreciation to Prof. Dr. H. Nevzat Özgüven and Assoc. Prof. Dr. Erhan Budak for their excellent supervision, valuable advices and guidance throughout all stages of this study.

Thanks are also due to research assistant Mr. Alper Ertürk for his effort in analytical modeling of the subassemblies and for his contribution and criticisms in the development of the proposed method. Also thanks are due to technician Mr. Mehmet Güler of the Sabanci University for his help in the preparation of the experimental set up.

Special acknowledgements are due to the author's family for their support during this work. He also offers his appreciation to his housemates for their support and patience.

This work is also supported by Scientific and Technological Research Council of Turkey (TUBITAK) under the project number 104M430.

Table of Contents

LIST OF TABLES

TABLES

LIST OF FIGURES

FIGURES

LIST OF SYMBOLS

SYMBOLS

c_{yf}	: Linear displacement – to – force damping
c_{ym}	: Linear displacement – to – moment damping
$c_{\theta f}$	: Angular displacement – to – force damping
$c_{\theta m}$	: Angular displacement – to – moment damping
f	: Activation function at the hidden layer
H_{mn}	: Receptance function (Linear displacement at point m due to the unit harmonic force excitation at point n)
k_{ym}	: Linear displacement – to – moment stiffness
k_{yf}	: Linear displacement – to – force stiffness
$k_{\theta f}$	: Angular displacement – to – force stiffness
$k_{\theta m}$	: Angular displacement – to – moment stiffness
L_{mn}	: Receptance function (Linear displacement at point m due to the unit harmonic moment excitation at point n)
N_{mn}	: Receptance function (Angular displacement at point m due to the unit harmonic force excitation at point n)
P_{mn}	: Receptance function (Angular displacement at point m due to the unit harmonic moment excitation at point n)
ω	: Excitation frequency

w_{ij} : Weight between i^{th} neuron of input layer and j^{th} neuron of hidden layer

w_{jk} : Weight between j^{th} neuron of hidden layer and k^{th} neuron of output layer

η : Learning rate of the neural network

CHAPTER 1

INTRODUCTION

1.1 Literature Survey

Machining is one of the most commonly used manufacturing processes in variety of industries. Majority of the machining operations are carried out on machining centers due to their capability to produce wide variety of parts. In machining centers, chatter is the main source of process instability which results in poor surface finish and low material removal rate. Chatter results from the dynamic interaction between the cutting process and the structures which may yield instability. With the increasing trends in high precision machining, chatter has become an important problem in machining processes. In order to decrease the effects of chatter, mechanism of the cutting process is examined in detail for decades [1-5] and the stability lobe diagram method, which provides the stable regions in the machining process for the depth of cut and spindle speed combinations, has been developed [3-6]. Although there are various methods for the generation of stability diagrams, in all approaches the identification of tool point Frequency Response Function (FRF) of the spindle – holder – tool assembly is required. In general, the tool point FRF is determined experimentally using impact testing and modal analysis. In impact tests, the tool point FRF is obtained with exciting the assembly at the tool tip with an instrumented hammer which also measures the impact force, and measuring the response with an accelerometer at the tool tip. After these measurements, tool tip FRF is calculated using the frequency spectrums of the force and the response. In this approach, for every

combination of spindle, holder and tool the modal testing must be performed, which is time consuming and may be costly especially on production machines. This has lead researchers to investigate alternative methods to obtain tool point FRF. Schmitz et al. [7-9] proposed a semi – analytical method which applies the receptance coupling technique to couple the experimentally obtained spindle – holder subassembly receptances with the analytically obtained tool receptances using the contact parameters at the holder tool interface.

Schmitz's semi - analytical method in determining the tool point FRF has been followed by several studies based on receptance coupling method. [10-12]. Recently, Ertürk et al. [13] proposed an experimentally verified [13,14] analytical model for predicting the tool point FRF by combining the receptance coupling and structural modification techniques where all components of the spindle-holder-tool assembly were modeled analytically with the Timoshenko beam theory and combined with the contact parameters at the spindle – holder and holder – tool interfaces.

After all improvements, studies showed that the accurate calculation of tool point FRF highly depends on the accuracy of contact parameters at the spindle – holder and holder – tool interfaces. Therefore, some of the recent studies concentrated on the contact parameters. Schmitz et al. [15] introduced off-diagonal elements to the diagonal joint stiffness matrix used in their early work [7-9] to account for the translations imposed by moments and rotations caused by forces. More recently, Ahmadi and Ahmadian [16] considered the holder-tool interface as a distributed elastic layer to model the change in the normal contact pressure along the joint interface. Although the methods of modeling the contact mechanism at spindle – holder and tool – holder interfaces were improved, the identification of the contact parameters were limited to numerical optimization techniques in all of these studies. In this approach, tool point FRF of the spindle – holder – tool assembly is

modeled analytically or semi analytically and compared with the measured tool point FRF. Finally, the contact parameters are identified by fitting the analytical tool point FRF to the experimentally obtained tool point FRF using nonlinear least square error minimization (NLSEM). The main uncertainty in NLSEM technique is the convergence behavior of the identified contact parameters. Depending on the initial values of the contact parameters, the numerical solution using NLSEM converges to different values. Therefore, different sets of solutions are obtained for the contact parameters where it is impossible to identify the correct ones. This behavior is due to the nonlinearity of the LSEM approach. It is not uncommon to obtain more than one solution since the numerical solution may converge to the results for a local minimum. Thus, mathematically meaningful but physically meaningless results may be obtained. However, the effect analysis performed by Ertürk et al. [17] showed that the contact parameters at the spindle – holder interface mainly affect the first elastic mode and contact parameters at the holder – tool interface mainly affect the second elastic mode. In addition to these observations it is also concluded that the stiffness values at the interface points alter the modal frequencies, and damping values alter the magnitude of the FRF peaks.

The reason why the identification of contact parameters at the interface points of machining centers is concentrated on experimental techniques is mainly the complexity of the contact mechanisms. Although Hertz contact theory provides approximate calculations of contact mechanisms in various contact cases, e.g. cylindrical and tapered type contacts, it may not be used in some cases since Hertz contact theory is derived for the cases where the contact area is small in relation to the curvature of contacting bodies [18]. Rivin [18] proposed semi - analytical methods for the determination of stiffness values in machining centers, however there is still need for experiments in order to identify some coefficients. In addition, Rivin's semi – analytical model for the determination of contact

parameters is limited to the contact stiffness identification, but they cannot be used for the determination of contact damping.

In order to eliminate the dependency on experimentation in identification of contact parameters, recent studies showed that neural networks can also be an effective tool. Liu and Ewins [19] used neural network for identification of joint dynamic parameters and Kang et Al. [20] used neural networks in the stiffness identification of angular contact ball bearings. It is obvious that the main difficulty in using neural networks to identify the contact parameters is obtaining a reliable training set. Because, in order to get successful results from the neural network, it should be trained with reliable input parameters. However there does not exist an accurate method for the identification of contact parameters. Therefore, before the training of neural networks, identification problem of the contact parameters should be solved.

1.2 Objective

The aim of this thesis is to investigate the contact parameters at different interface surfaces of machining centers, and to develop identification methods for them. Since there is no fast and accurate way of identifying these parameters, such a developed method can make a significant contribution to the accurate prediction of tool point FRFs, and thus to the generation of stability diagrams in order to avoid chatter. In addition to the identification problem, this thesis is also concentrated on the elimination of experimental dependency for each case through application of the artificial neural networks. Therefore, the developed methods can make it possible to obtain tool point FRFs without experimentation for each case.

1.3 Scope of the Thesis

Outline of the thesis is as follows:

In Chapter 2, the theory of the contact parameter identification formulation and the improvements made in the closed form approach are presented. For this purpose, forward receptance coupling equation is rearranged, and a closed form expression for the contact parameter identification is obtained. As an improvement fully populated complex stiffness matrix is used in the formulation, and to overcome the practical application problems to measure rotational degree of freedom (RDOF) related FRFs, they are obtained with finite difference method. Then the approach developed is verified first with simulated case studies in this chapter. Moreover, the proposed method is tested with the polluted receptance matrices and the effect of the noise in the input parameters is studied in detail.

In Chapter 3, experimental verification of the proposed method is presented. For this purpose, displacement to force receptances of the spindle- holder subassembly and spindle-holder-tool assembly are obtained with the modal testing, and remaining rotational degree of freedom (RDOF) related receptances are obtained by the finite difference method. Also, in order to minimize the noise effect of the measurements, experimentally obtained receptances are filtered with Savitzky Golay filter [21]. After the determination of the receptance matrices, the identification is performed with the proposed method and unique contact parameters are identified from the dominant tool mode region. Finally, the identified parameters are used in the forward receptance coupling equation, and it is concluded that the proposed method can be used for the identification of contact parameters.

In Chapter 4, in order to eliminate the experimental dependency, artificial neural networks are studied. For that purpose, for different combinations of tool gauge

length and tool diameter, contact parameters are identified and are used in the training of the neural networks. Finally, the trained neural network is tested with the first seen inputs, and it is observed that the neural networks can learn the characteristics of the contact mechanism accurately and thus can successfully be used in the identification of contact parameters.

In Chapter 5, possible inaccuracies of the accelerometer measurements are examined. For this purpose, comparison of laser doppler vibrometer (LDV) and accelerometer measurements are presented and the mass effect of the accelerometers is expressed. After that, a structural modification with matrix inversion method is applied in order to eliminate the mass effect. With the modification technique, consistent results with the laser measurements are obtained.

In Chapter 6, summary and conclusion of the thesis is given. Also, scope of a possible future work is suggested.

Chapter 2

A CLOSED FORM APPROACH IN IDENTIFICATION OF CONTACT PARAMETERS

2.1 Mathematical Background

Components of a typical spindle – holder – tool assembly and contact parameters used in the receptance coupling are shown in Figure 2.1. In order to obtain the tool point FRF of a spindle – holder – tool assembly given in Figure 2.1 analytically, the model proposed by Ertürk et al. [13] provides an efficient method. In this model, individual receptance matrices of the subassemblies spindle (*S*), holder (*H*) and tool are obtained by rigid receptance coupling of free-free Timoshenko beams. After obtaining subassembly receptance matrices, the spindle and holder are coupled through complex stiffness matrix $[K_{sh}]$ at the spindle-holder interface and the spindle – holder subassembly tip point receptance matrix is obtained as follows:

$$[SH_{11}] = [H_{11}] - [H_{12}]\left[[H_{22}] + [K_{sh}]^{-1} + [S_{11}]\right]^{-1}[H_{21}] \tag{2.1}$$

Finally, spindle – holder subassembly receptance matrices are coupled with the tool receptances through complex stiffness matrix $[K_{ht}]$ at the holder-tool interface, and the receptance matrix of the spindle – holder – tool assembly is obtained as follows:

$$[SHT_{11}] = [T_{11}] - [T_{12}]\left[[T_{22}] + [K_{ht}]^{-1} + [SH_{11}]\right]^{-1}[T_{21}] \tag{2.2}$$

Receptance matrices given in Equation (2.1) and Equation (2.2) are 2×2 matrices corresponding to translational and rotational degrees of freedom (DOF). Subscripts 11 and 22 represent point receptances and 12 and 21 represent cross receptances.

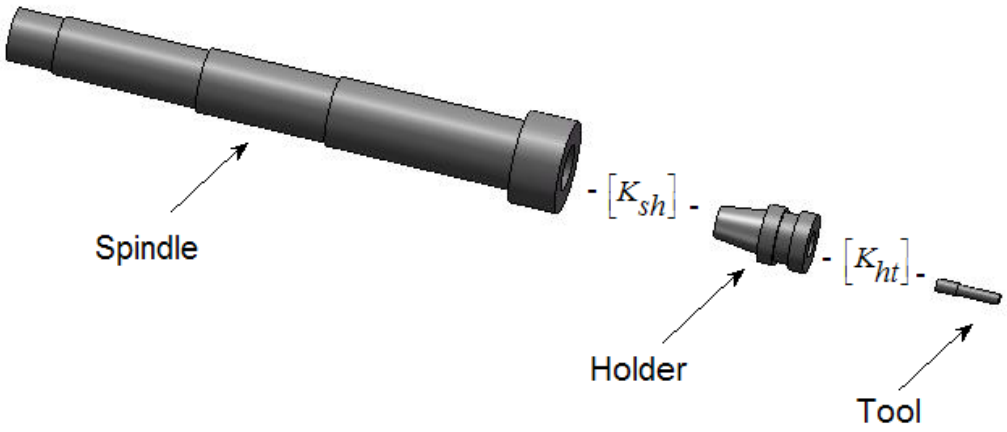

Figure 2.1 Components of spindle-holder-tool assembly and the complex stiffness matrices of spindle-holder and holder-tool interfaces.

Since the contact mechanism is complicated and difficult to model at the spindle – holder and holder – tool interface with analytical methods, the part of the holder inside the spindle is coupled to the spindle rigidly, and the remaining part outside the spindle is coupled with spindle (which already includes the part of the holder inside the spindle) through complex stiffness matrix. Similarly, for the holder –

tool contact, the part of the tool inside the holder and collet are coupled to the holder rigidly, and the remaining part of the tool is coupled with holder (which already includes part of the tool inside the holder) through complex stiffness matrix. Therefore, in Equations (2.1) and (2.2), *S* represents the spindle and holder part inside the spindle, and *SH* represents spindle, holder and part of the tool in the holder assembly.

In the following section, these elastic receptance coupling equations are rearranged for obtaining closed-form expressions to predict the complex stiffness matrices of holder-tool and spindle-holder interfaces. Thus, the dynamical contact parameters, i.e. stiffness and damping parameters, of these interfaces can be extracted in closed-form.

2.2 Identification of Contact Dynamics at the Holder-Tool Interface

2.2.1 Rearrangement of Receptance Coupling Equations

In order to obtain a closed form expression for the contact parameters, receptance coupling equations can be rearranged as expressed by Özşahin et al [22]. For the holder – tool contact parameters, in Equation (2.2) if the spindle – holder subassembly and tool receptances are taken to the right hand side of the equation, a closed form equation given below can be obtained.

$$[K_{ht}] = \left[\left[[T_{12}]^{-1} \left[[T_{11}] - [SHT_{11}] \right] [T_{21}]^{-1} \right]^{-1} - [T_{22}] - [SH_{11}] \right]^{-1} \tag{2.3}$$

In the early stage application of receptance coupling theory in stability diagram determination, the complex stiffness matrix given below was used in the elastic receptance coupling equations:

$$[K_{ht}] = \begin{bmatrix} k_y^{ht} + i\omega c_y^{ht} & 0 \\ 0 & k_\theta^{ht} + i\omega c_\theta^{ht} \end{bmatrix} \tag{2.4}$$

In Equation (2.4), off-diagonal elements which are linear displacement-to-moment and angular displacement-to-force terms, are neglected. In a recent study, Schmitz et al. [15] replaced this classical form of the joint stiffness matrix with the following fully populated matrix:

$$[K_{ht}] = \begin{bmatrix} k_{yf}^{ht} + i\omega c_{yf}^{ht} & k_{ym}^{ht} + i\omega c_{ym}^{ht} \\ k_{\theta f}^{ht} + i\omega c_{\theta f}^{ht} & k_{\theta m}^{ht} + i\omega c_{\theta m}^{ht} \end{bmatrix} \tag{2.5}$$

where k_{yf}^{ht} is the linear displacement – to – force stiffness, c_{yf}^{ht} is the linear displacement – to – force damping, k_{ym}^{ht} is the linear displacement – to – moment stiffness, c_{ym}^{ht} is the linear displacement – to – moment damping, $k_{\theta f}^{ht}$ is the angular displacement – to – force stiffness, $c_{\theta f}^{ht}$ is the angular displacement – to – force damping, $k_{\theta m}^{ht}$ is the angular displacement – to – moment stiffness and $c_{\theta m}^{ht}$ is the angular displacement – to – moment damping of the holder-tool interface, ω is the excitation frequency and i is the unit imaginary number.

Although complex stiffness matrix proposed in Equation (2.5) has non- zero off diagonal terms, it is expected that these terms should be equal or close to each other so that the linear receptance coupling formulation is in agreement with the Betti-Maxwell reciprocity theorem of linear elasticity [23]. Otherwise, the forward receptance coupling formulation given by Equation (2.2) may yield an asymmetric

tool point receptance matrix even for symmetric subsystem matrices, violating the aforementioned theorem. Therefore, after the identification process, one should check the symmetry.

As seen from Equation (2.3), in order to perform the identification method to obtain the contact parameters, tool receptance matrices, and spindle – holder subassembly tip point receptance matrix and spindle – holder – tool assembly tool point receptance matrix should be obtained. Methods applied for the receptance matrices of tool are given in the following section. For the spindle – holder subassembly and spindle – holder – tool assembly tip point receptance matrices, applied methods are given in section 2.2.3.

2.2.2 Analytical Calculation of Tool Receptance Matrices

In order to obtain tool point FRF of spindle – holder – tool assembly, receptance matrices of the cutting tool in free-free boundary conditions should be obtained which are denoted by $[T_{11}]$, $[T_{12}]$, $[T_{21}]$ and $[T_{22}]$ in Equation (2.2). These point and cross receptances of the cutting tool are given as follows:

$$[T_{11}]=\begin{bmatrix} H_{11}^t & L_{11}^t \\ N_{11}^t & P_{11}^t \end{bmatrix}, \quad [T_{12}]=\begin{bmatrix} H_{12}^t & L_{12}^t \\ N_{12}^t & P_{12}^t \end{bmatrix}$$
$$[T_{21}]=\begin{bmatrix} H_{21}^t & L_{21}^t \\ N_{21}^t & P_{21}^t \end{bmatrix}, \quad [T_{22}]=\begin{bmatrix} H_{22}^t & L_{22}^t \\ N_{22}^t & P_{22}^t \end{bmatrix} \tag{2.6}$$

where;

$$H_{mn}=\frac{w_m}{f_n}\ ,\ N_{mn}=\frac{\theta_m}{f_n}\ ,\ L_{mn}=\frac{w_m}{m_n}\ ,\ P_{mn}=\frac{\theta_m}{m_n} \tag{2.7}$$

In Eqn. (2.7), w is the transverse displacement θ is the bending slope, *f* is the transverse force, *m* is the bending moment and the subscripts stand for the points of interest over the length of the tool. For instance, if the tool is to be modeled as a uniform beam, the elements of its point receptance matrix $[T_{11}]$ are given as follows [13]:

$$H_{11}^{t} = \frac{-1}{\rho AL\omega^2} + \frac{-3}{\rho AL\omega^2} + \sum_{r=1}^{\infty} \frac{\phi_r(L)\phi_r(L)}{(1+i\gamma)\omega_r{}^2 - \omega^2} \tag{2.8}$$

$$N_{11}^{t} = \frac{-6}{\rho AL^2\omega^2} + \sum_{r=1}^{\infty} \frac{\phi_r'(L)\phi_r(L)}{(1+i\gamma)\omega_r{}^2 - \omega^2} \tag{2.9}$$

$$L_{11}^{t} = \frac{-6}{\rho AL^2\omega^2} + \sum_{r=1}^{\infty} \frac{\phi_r(L)\phi_r'(L)}{(1+i\gamma)\omega_r{}^2 - \omega^2} \tag{2.10}$$

$$P_{11}^{t} = \frac{-12}{\rho AL^3\omega^2} + \sum_{r=1}^{\infty} \frac{\phi_r'(L)\phi_r'(L)}{(1+i\gamma)\omega_r{}^2 - \omega^2} \tag{2.11}$$

where ρ is the density, *A* is the cross-sectional area, *L* is the length and γ is the loss factor of the tool. Furthermore, ω_r is the *r*-th natural frequency, $\phi_r(x)$ is the *r*-th mode shape for transverse displacement of the tool and $\phi_r'(x)$ is the derivative of $\phi_r(x)$ with respect to axial independent displacement variable *x*.

2.2.3 Calculation of Rotational Degree of Freedom Related FRF with Finite Difference Method

In addition to tool point and cross receptances, spindle – holder subassembly and spindle – holder – tool assembly receptances should also be calculated as given in Equation (2.3). For the spindle – holder – tool assembly receptance matrix, first element of the matrix which is H_{11}^{sht} can be obtained by performing impact testing. But for the remaining receptances, simple impact testing is not applicable due to

the difficulty in measuring angular displacements and exciting the system with moment. Therefore, approximate methods can be applied for the Rotational Degree of Freedom (RDOF) related receptances L_{11}^{sht}, N_{11}^{sht} and P_{11}^{sht}. For the approximate solution Duarte and Ewins proposed a finite difference method [24].

In the proposed method first or second order methods exist. In the first order finite difference method, forward and backward transformation matrices are given by the following equations, respectively:

$$\left[T_{1f}\right]=\begin{bmatrix}0 & 1\\ 1/s & -1/s\end{bmatrix} \tag{2.12}$$

$$\left[T_{1b}\right]=\begin{bmatrix}0 & 1\\ -1/s & 1/s\end{bmatrix} \tag{2.13}$$

where s represents the spacing between measurement points.

For the second order finite difference method, forward, central and backward transformation matrices are also given by the following equations, respectively:

$$\left[T_{2f}\right]=\frac{1}{2s}\begin{bmatrix}0 & 0 & 2s\\ -1 & 4 & -3\end{bmatrix} \tag{2.14}$$

$$\left[T_{2c}\right]=\frac{1}{2s}\begin{bmatrix}0 & 2s & 0\\ -1 & 0 & 1\end{bmatrix} \tag{2.15}$$

$$\left[T_{2b}\right]=\frac{1}{2s}\begin{bmatrix}0 & 0 & 2s\\ 1 & -4 & 3\end{bmatrix} \tag{2.16}$$

In finite difference method, according to the location where the RDOF related FRFs are desired, displacement-to-force cross and point FRFs are measured. If the second order approximation is preferred, measurements are taken from 3 distinct locations and if the first order approximation is preferred, measurements are performed at 2 distinct locations. Finally RDOF related FRFs are obtained as follows with the suitable transformation matrix to the order of approximation.

$$\left[H_{est}\right]=\begin{bmatrix} H_{yy} & H_{\theta y}^{T} \\ H_{\theta y} & H_{\theta\theta} \end{bmatrix}=\left[T\right]\left[H_{meas}\right]\left[T\right]^{T} \tag{2.17}$$

$$\left[H_{meas}\right]=\begin{bmatrix} h_{33} & h_{23} & h_{13} \\ h_{23}^{T} & h_{22} & h_{12} \\ h_{13}^{T} & h_{12}^{T} & h_{11} \end{bmatrix} \tag{2.18}$$

Most crucial part of the approximation method is that the accuracy of the method is highly dependent on the order of the approximation and spacing between measurement points. As expressed by Duarte and Ewins [24], higher order approximation requires smaller spacing between measurement points for the angular displacement – to – force FRFs and requires larger spacing for the angular displacement to moment FRFs. Therefore, for the four receptance matrices that define matrix $\left[SHT_{11}\right]$, one should carefully perform the experimental measurements on the cutting tool of the assembly so that H_{11}^{sht}, L_{11}^{sht}, N_{11}^{sht} and P_{11}^{sht} are obtained by a suitable approximation method and $\left[SHT_{11}\right]$ can be constructed. It is also required to obtain the receptance matrix $\left[SH_{11}\right]$ of the spindle-holder subassembly (without the cutting tool outside the holder) experimentally. The procedure of obtaining the elements of this matrix is similar to that used for generating $\left[SHT_{11}\right]$.

Having obtained all the receptance matrices at the right hand side of Equation (2.3) analytically and experimentally, one can obtain the complex stiffness matrix of the holder-tool joint, elements of which give the stiffness and damping parameters of the holder-tool interface: k_{yf}^{ht}, c_{yf}^{ht}, k_{ym}^{ht}, c_{ym}^{ht}, $k_{\theta f}^{ht}$, $c_{\theta f}^{ht}$, $k_{\theta m}^{ht}$, $c_{\theta m}^{ht}$.

2.3 Analytical Case Study

In this section an analytical case study for the identification method proposed is given. In order to apply the proposed method for an analytical case; spindle, holder and tool are modeled analytically. After obtaining the subassembly receptances, these receptances are coupled with the contact parameters at the spindle – holder and holder – tool interfaces given in Table 2.1 and Table 2.2, respectively.

As seen from Table 2.1 and Table 2.2, due to the symmetry requirement of the receptance matrices as discussed in section 2.2.1, off – diagonal terms of the complex stiffness matrices are taken to be equal.

Table 2.1 Dynamical contact parameters at the spindle - holder interface in the analytical case study

Linear displacement – to – force stiffness (N/m)	1.3×10^{7}
Linear displacement – to – force damping (N.s/m)	5
Linear displacement – to - moment stiffness (N.m/m)	6.06×10^{6}
Linear displacement – to – moment damping (N.m.s/m)	12.2
Angular displacement – to – force stiffness (N/rad)	6.06×10^{6}
Angular displacement – to – force damping (N.s/rad)	12.2
Angular displacement – to – moment stiffness (N.m/rad)	1.5×10^{4}
Angular displacement – to – moment damping (N.m.s/rad)	1

Table 2.2 Dynamical contact parameters at the holder-tool interface in the analytical case study

Linear displacement – to – force stiffness (N/m)	4.19×10^{7}
Linear displacement – to – force damping (N.s/m)	54
Linear displacement – to - moment stiffness (N.m/m)	2.06×10^{6}
Linear displacement – to – moment damping (N.m.s/m)	22.2
Angular displacement – to – force stiffness (N/rad)	2.06×10^{6}
Angular displacement – to – force damping (N.s/rad)	22.2
Angular displacement – to – moment stiffness (N.m/rad)	6.5×10^{4}
Angular displacement – to – moment damping (N.m.s/rad)	1

The tip point receptance of the spindle - holder subassembly (without the tool outside the holder) is obtained by coupling analytically obtained spindle and holder receptances by using the analytical model [13]. The first element of the receptance matrix $\left[SH_{11}\right]$ calculated is given in Figure 2.2.

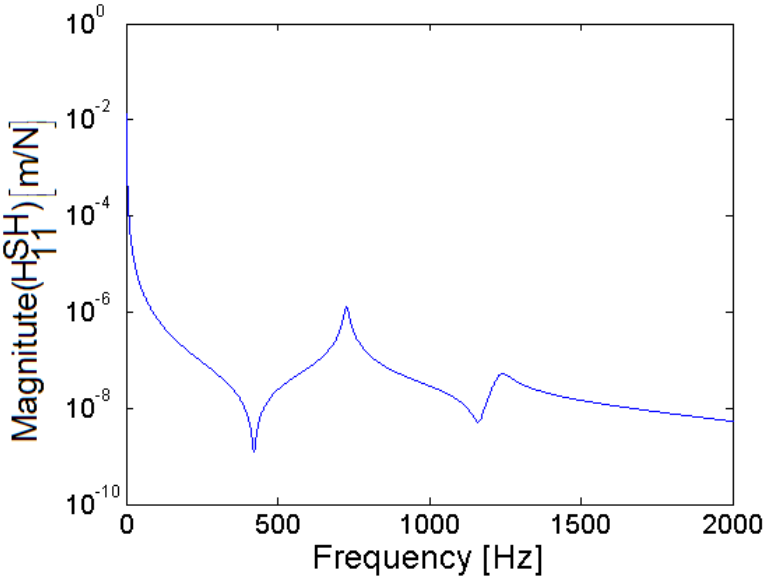

Figure 2.2 The analytically obtained tip point FRF (H_{11}^{SH}) of the spindle-holder subassembly.

The tool point FRF of the assembly is obtained by coupling the spindle – holder subassembly receptance matrix with tool receptances through complex stiffness matrix at the holder – tool interface. Tool point FRF which is the first element of the assembled matrix $\left[SHT_{11}\right]$ is given in Figure 2.3.

After obtaining the receptance matrices at the right hand side of Equation (2.3), complex stiffness matrix, and therefore the linear displacement – to – force, linear displacement – to – moment, angular displacement – to – force and angular displacement – to – moment stiffness and damping values can be identified. As can be seen from Figure 2.4 and Figure 2.5, the dynamic contact parameters of the holder-tool interface are exactly the same as the values entered as input to the analytical model (Table 2.2).

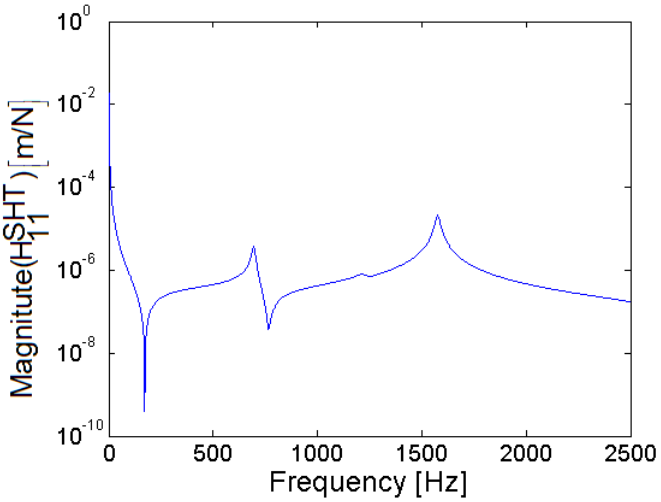

Figure 2.3 Analytically obtained tool point FRF (H_{11}^{SHT}) of the spindle-holder-tool assembly.

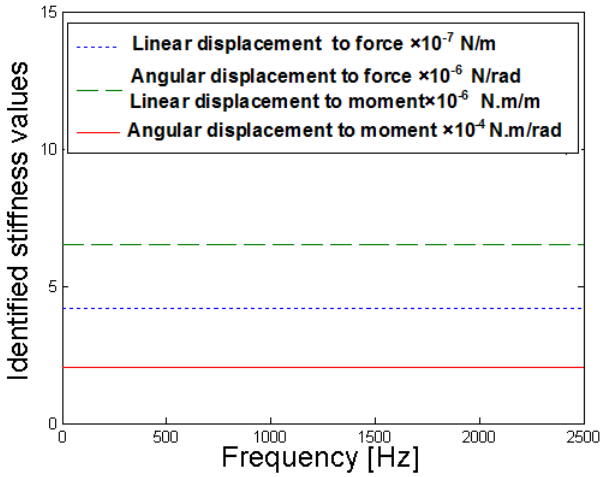

Figure 2.4 Identified stiffness values at the holder-tool interface obtained from Equation (2.3) by using the analytically obtained FRFs.

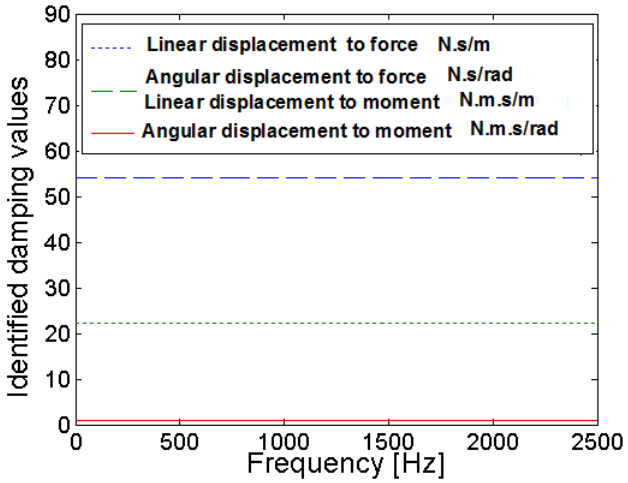

Figure 2.5 Identified damping values at the holder-tool interface obtained from Equation (2.3) by using the analytically obtained FRFs.

Since the FRFs constructed by the analytical model are directly used in the identification method of the dynamical contact parameters at the holder-tool interface, exactly the same values used as input are obtained. In order to simulate a more realistic scenario, random number arrays with mean value of unity and standard deviation of 5% are generated in MATLAB® and they are multiplied with the FRFs of matrices $\left[SH_{11}\right]$ and $\left[SHT_{11}\right]$. This way, the analytical coherence between the elements of these matrices is distorted. The distorted displacements to force FRFs are given in Figure 2.6 and Figure 2.7 respectively.

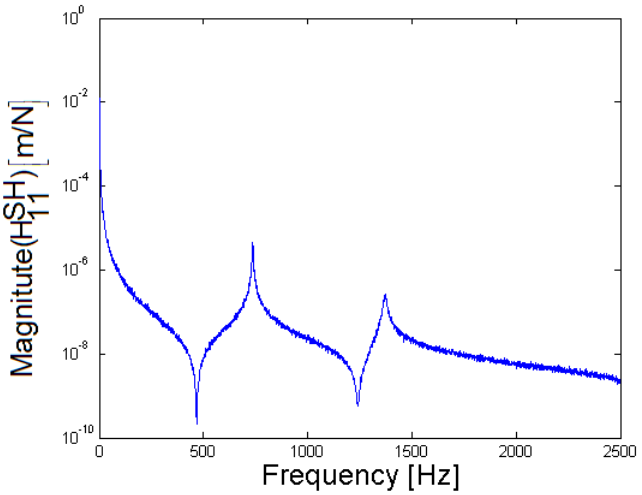

Figure 2.6 Distorted tip point FRF (H_{11}^{SH}) of the spindle-holder subassembly.

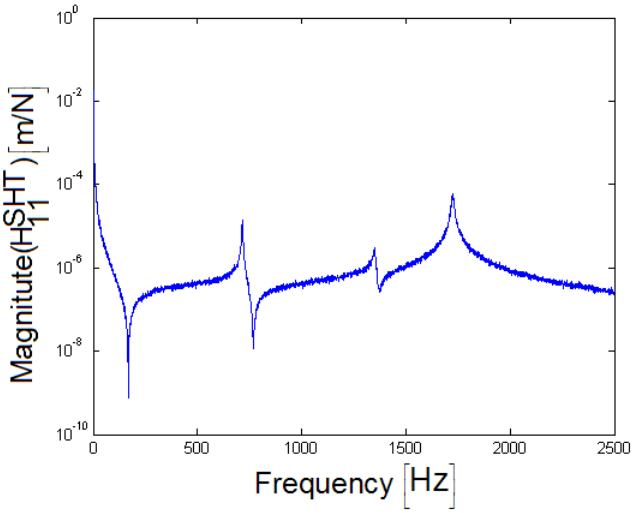

Figure 2.7 Distorted tip point FRF (H_{11}^{SHT}) of the spindle – holder - tool assembly.

Since in the proposed method the tool receptances can be obtained analytically, only the first elements of the spindle – holder subassembly and spindle – holder – tool assembly receptances are polluted. Then, the stiffness and damping parameters of holder-tool interface are obtained and linear displacement – to – force stiffness and linear displacement – to – force damping are plotted against frequency in Figure 2.8 and Figure 2.9, respectively.

For the remaining contact parameters, similar deficiencies are observed as in the Figure 2.8 and Figure 2.9. Comparing the fully analytical case and distorted case, deficiencies in the identified contact parameters show that the proposed method is highly sensitive to noise in the input receptances. This sensitivity is mainly the result of the matrix inversions used in the calculations. Although the identified parameters with frequency are not constants as can be seen from Figure 2.8 and Figure 2.9, in the effect analysis study [17] it is shown that the holder-tool interface controls mainly the tool mode of the tool point FRF. Consistent with the effect analysis results [17], as seen from Figure 2.8b and Figure 2.9b, the identified stiffness and damping parameters are not affected from the noise in input receptance values in the tool mode region. In the tool mode region, mean value of the identified stiffness is 4.05×10^7 N/m and the mean value of the identified damping is 51 N.s/m. Therefore, instead of considering the whole frequency band one should focus on the vicinity of the tool mode frequency and identify the interface parameters of the holder-tool interface from that region. Consequently, the translational stiffness and damping parameters are identified in Figure 2.8 and Figure 2.9 at the frequency of the second vibration mode, and they are found in good agreement with those identified in Figure 2.4 and Figure 2.5.

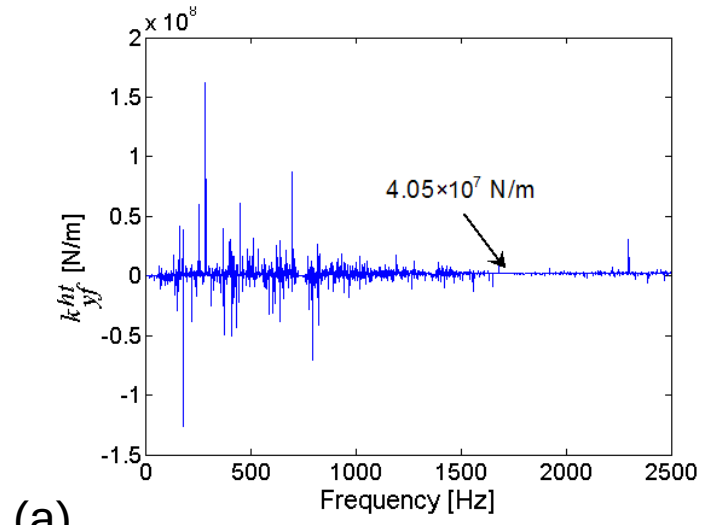

(a)

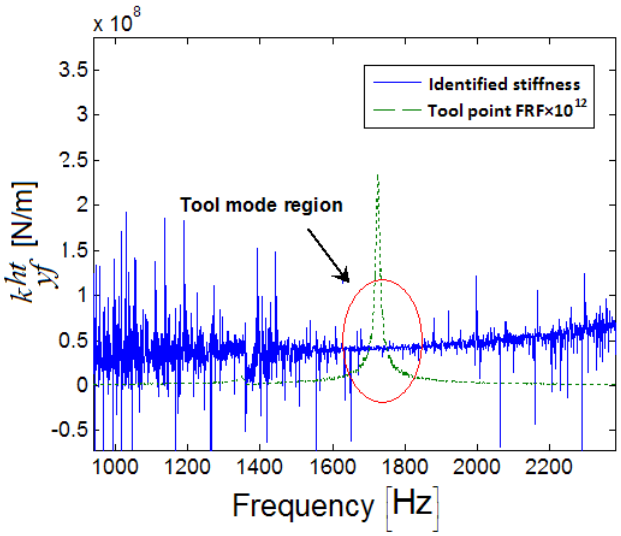

(b)

Figure 2.8 (a) Identified displacement to force stiffness, (b)Identified displacement to force stiffness and tool point FRF at the tool mode region.

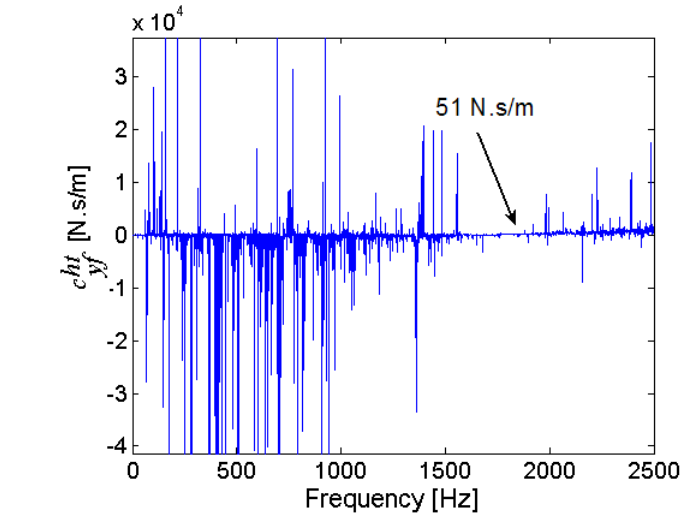

(a)

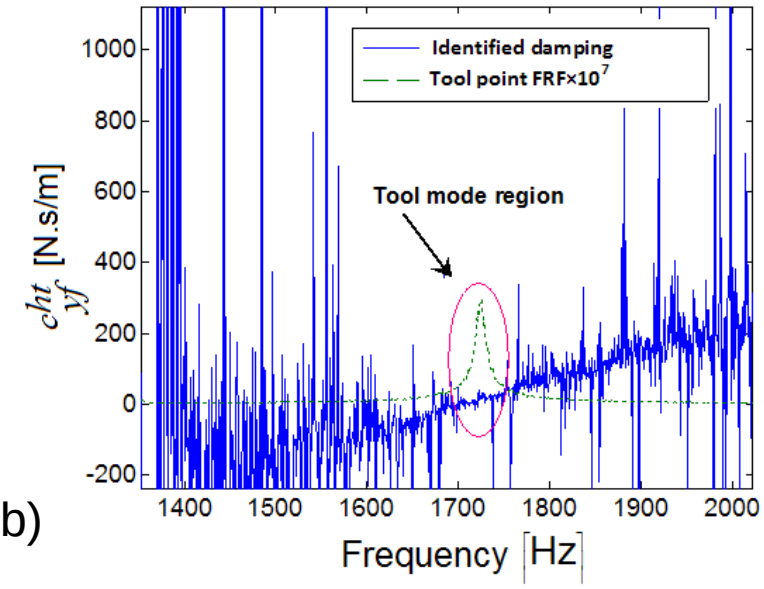

(b)

Figure 2.9 (a) Identified displacement to force damping, (b) Identified displacement to force damping and tool point FRF at the tool mode region.

Chapter 3

EXPERIMENTAL VERIFICATION FOR IDENTIFICATION OF CONTACT DYNAMICS AT THE HOLDER-TOOL INTERFACE

3.1 Introduction

In cutting stability analysis, the tool point FRF must be known. Although important progress has been achieved in modeling the spindle – holder – tool assembly analytically, measurements are still needed since there are no analytical methods for the prediction of contact parameters. Recent studies have shown that accurate identification of contact parameters plays a crucial role in accurate determination of tool point FRFs. Therefore, the accuracy of the experimentation becomes very important. In this chapter, in order to investigate the contact parameters at the spindle – holder and holder – tool interface, experimental investigations are carried out using real machine tool components.

3.2 Experimental Setup

In order to perform experiments on real machine parts, BT 40 type holder is assembled to the free-free spindle and the tool is clamped to the holder via collets. Spindle and the BT40 type holder used in the assembly are shown in Figure 3.1 and Figure 3.2, respectively. Also, depending on the tool diameter different collets are used in the holder for clamping. These collets are also shown in Figure 3.3.

Figure 3.1 Spindle used in experiments.

Figure 3.2 BT40 type holder clamped to spindle.

As it can be seen from Figure 3.2 and Figure 3.3, the contacts between the spindle and the holder and the collet and holder are tapered types whereas the contact between the collet and the tool is cylindrical type.

The clamping torque applied on the holder during the installation of the tools was maintained at the same level since it may have an effect on the FRFs. A complete spindle – holder – tool assembly where 12 mm diameter tool is clamped to the holder is shown in Figure 3.4.

Figure 3.3 Collets used in experimental setup.

Figure 3.4 Spindle – holder – tool assembly used in experiments.

3.3 Modal testing and Measurement Equipment

In modal testing, the most common way of obtaining FRFs is the single point excitation where the system is excited at a single point, and the response is measured. In such experiments both response and excitation are measured simultaneously, and the FRF of the system is obtained from the measured values. In measuring system response, accelerometers are commonly used. For both exciting the system, and measuring the excitation level, impact hammers are used widely. Although accelerometers are common measurement devices, their mass

may affect the system response, and cause FRF peak values to shift to the left in the frequency range of interest. Therefore, in order to obtain accurate measurement results, experiments are performed by measuring the response using both accelerometer and LDV laser vibrometer. Measurement results from both sensors are compared. The accelerometer mass effect is investigated for accurate prediction of tool point FRF, and the results are given in chapter 5.

In addition to measurement techniques and devices, another important aspect of the modal testing is the boundary conditions of the system. Boundaries can be taken free or fixed according to the model used. In this thesis, since spindle – holder – tool assembly with free end conditions is modeled analytically, experiments are also performed with the same end conditions. But it is not very practical to support the experimental set up in real free end conditions, and it is often preferred to suspend the assembly in a manner which approximates the free end condition [25]. Therefore, the assembly is supported with elastic bands which behave as soft springs. Free free suspended spindle-holder-tool assembly is also given in Figure 3.5.

Figure 3.5 Free free suspended spindle-holder-tool assembly.

3.4 Experimental Case Study

In this section, in addition to the analytical case study given in section 2.3, an experimental case study for the identification approach is presented. Experiments were performed using the set up whose details are given in section 3.1. During experiments, a 16 mm diameter carbide tool of 123 mm length was clamped in the holder with an overhang length of 49 mm. The tool was clamped to the holder using 30 N.m clamping torque. By using the laser sensor, the mass loading effect of the accelerometers was avoided, and furthermore the accuracy of the measurements is improved.

Since in the analytical modeling tool part inside the holder is rigidly coupled to the holder and this tool part is included in the spindle-holder subassembly, experiments are also performed with the same configuration. For the spindle-holder subassembly, holder is attached to the spindle and just the tool part inside the holder is clamped to the holder. After obtaining subassembly, tip point receptance was determined using impact testing and the response is as shown in Figure 3.6. Note that this is the first element of the assembled matrix $\left[SH_{11}\right]$.

As observed in Section 2.2, the noise in the measured data highly affects the identification method. Therefore, the experimentally obtained FRFs are filtered with the Savitzky-Golay filter [21]. The filtered tip point FRFs of the spindle-holder subassembly is given also in Figure 3.7.

For the tool point FRF of the assembly, similar to spindle – holder subassembly, impact test was performed and obtained tool point FRF is shown Figure 3.8. Again, this is the first element of the assembled matrix $\left[SHT_{11}\right]$. The filtered tip point FRF of the spindle holder tool assembly is also given in Figure 3.9.

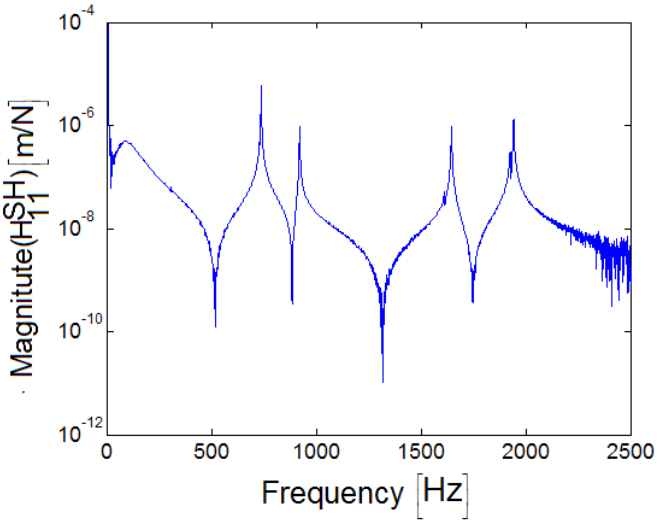

Figure 3.6 Experimentally obtained tip point FRF (H_{11}^{SH}) of the spindle-holder subassembly.

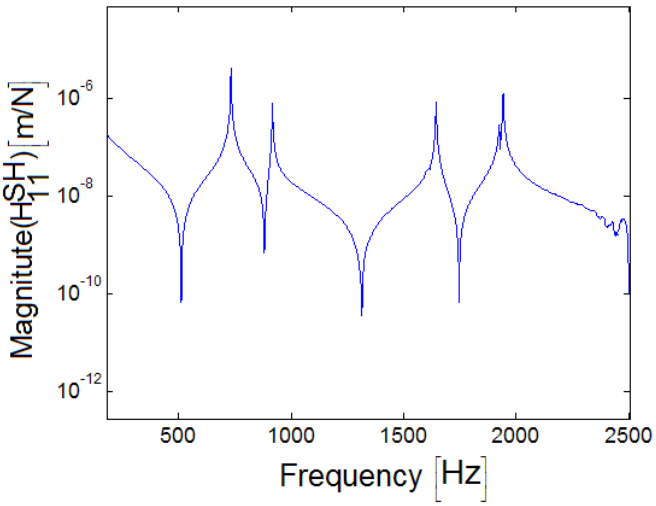

Figure 3.7 Filtered tip point FRF of the spindle holder subassembly.

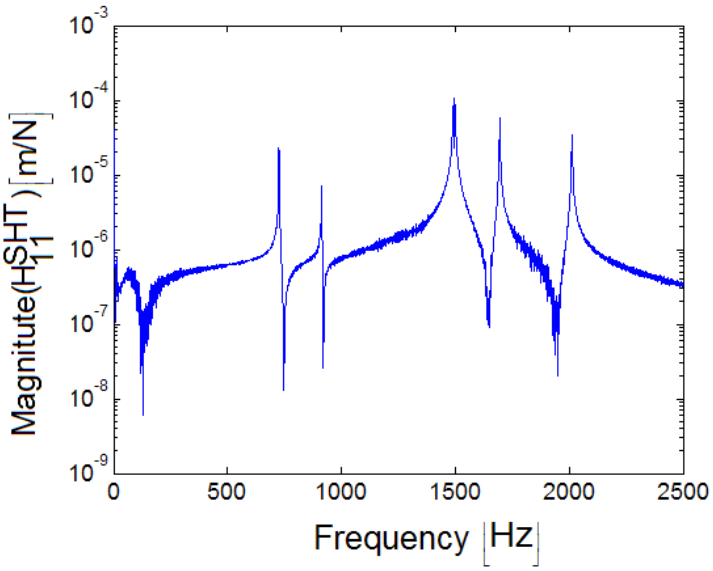

Figure 3.8 Experimentally obtained tool point FRF (H_{11}^{SHT}) of the spindle – holder - tool assembly.

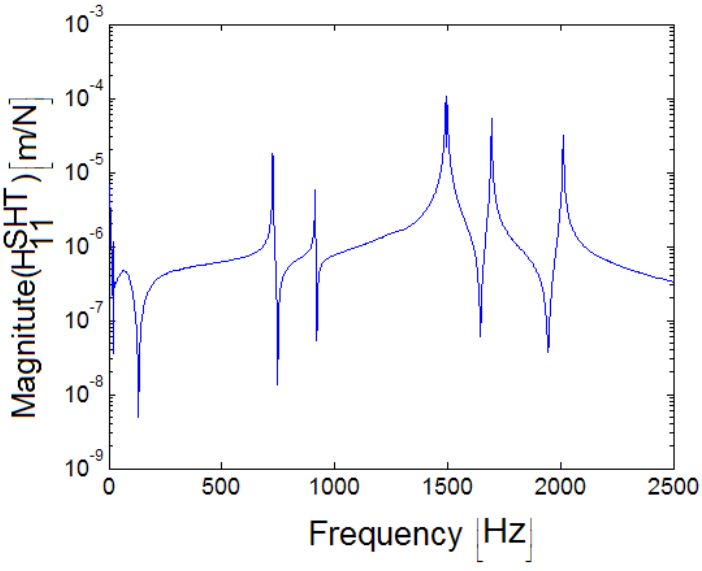

Figure 3.9 Filtered tip point FRF of the spindle – holder - tool assembly.

In order to obtain angular displacement or moment related FRFs of $[SH_{11}]$ and $[SHT_{11}]$, second order approximation proposed by Duarte and Ewins [26] is used with spacing of 35 mm and 40 mm between measurement points for the holder – spindle subassembly and spindle – holder – tool assembly, respectively. The resulting FRFs of the $[SH_{11}]$ which are L_{11}^{SH}, N_{11}^{SH} and P_{11}^{SH} are given in Figure 3.10 – Figure 3.12 respectively. Also resulting FRFs of the $[SHT_{11}]$ which are L_{11}^{SHT}, N_{11}^{SHT} and P_{11}^{SHT} are given in Figure 3.13 – Figure 3.15 respectively. It is important to note that the accuracy of the method depends on the spacing between measurement points and the order of the approximation [24].

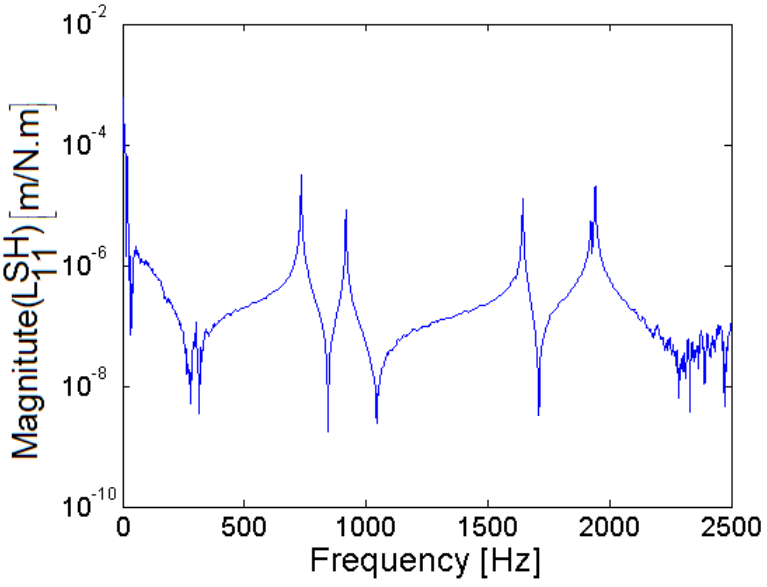

Figure 3.10 Approximately obtained tip point FRF (L_{11}^{SH}) of the spindle-holder subassembly.

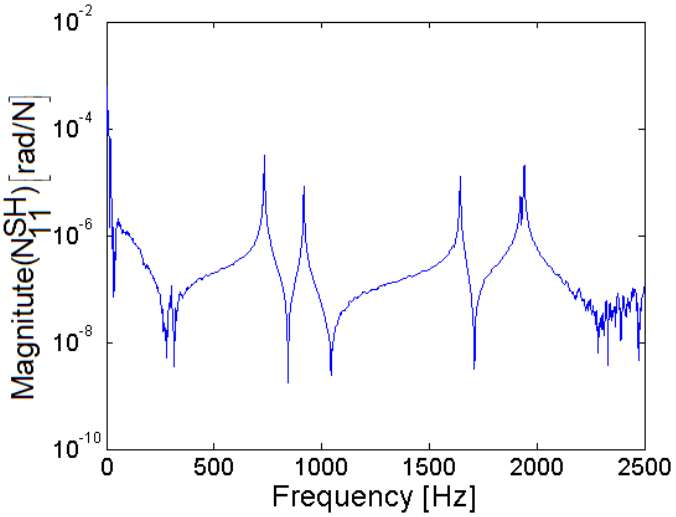

Figure 3.11 Approximately obtained tip point FRF (N_{11}^{SH}) of the spindle-holder subassembly.

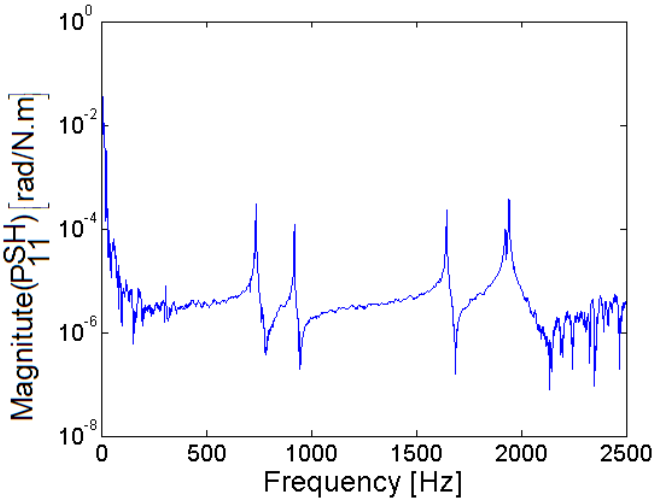

Figure 3.12 Approximately obtained tip point FRF (P_{11}^{SH}) of the spindle-holder subassembly.

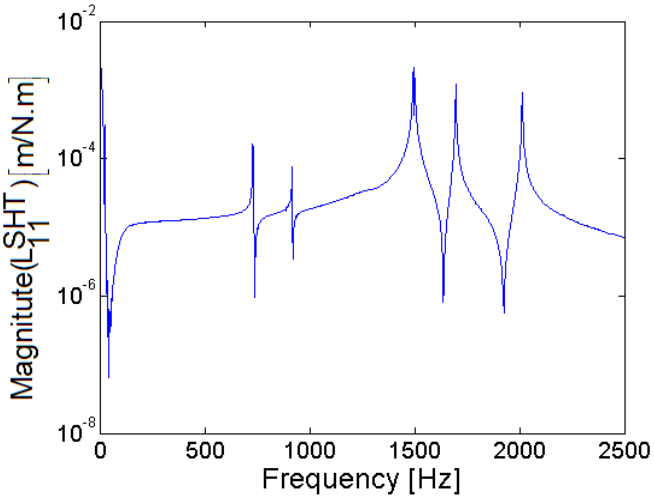

Figure 3.13 Approximately obtained tool point FRF (L_{11}^{SHT}) of the spindle-holder-tool assembly.

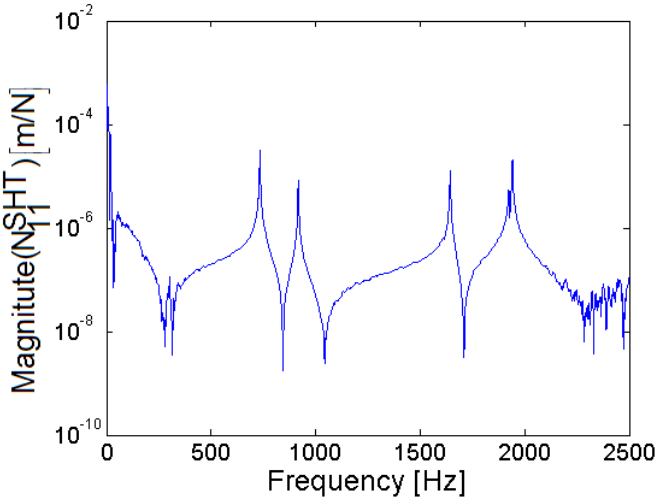

Figure 3.14 Approximately obtained tool point FRF (N_{11}^{SHT}) of the spindle-holder-tool assembly.

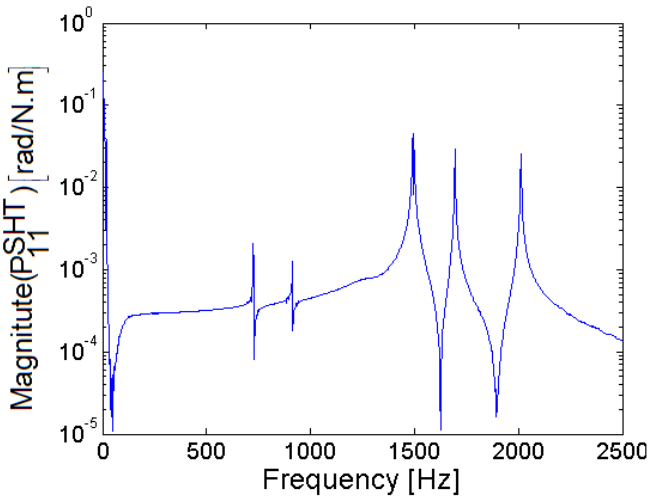

Figure 3.15 Approximately obtained tool point FRF (P_{11}^{SHT}) of the spindle-holder-tool assembly.

The receptance matrices of the cutting tool in free-free boundary conditions, which are denoted by $[T_{11}]$, $[T_{12}]$, $[T_{21}]$ and $[T_{22}]$ are obtained analytically. After obtaining the FRFs required for constructing the right hand side of Equation (2.3), the complex stiffness matrix $[K_{ht}]$ is obtained from Equation (2.3). Then, the linear displacement – to – force, linear displacement – to – moment, angular displacement – to – force and angular displacement – to – moment complex stiffness functions of the holder-tool interface are obtained.

It is known from the typical spindle-holder-tool assembly investigated by Ertürk et al. [17] that the holder – tool connection parameters mainly affect the tool-dominant vibration mode. Hence, it is reasonable to identify the holder- tool contact parameters from this mode. As seen from Figure 3.8, the tool point FRF of the assembly has 5 distinct modes in the frequency range of interest. Therefore, in

order to identify tool-dominant mode, the assembly tool point FRF is measured for different overhang lengths of the tool. The three different overhang lengths taken are 82 mm, 88 mm and 94 mm. For these three configurations, it is observed that the third mode is mainly affected by the tool overhang length as shown in Figure 3.16. Therefore, the third vibration mode in the tool point FRF is the tool mode and the holder-tool contact dynamics can be identified from this mode.

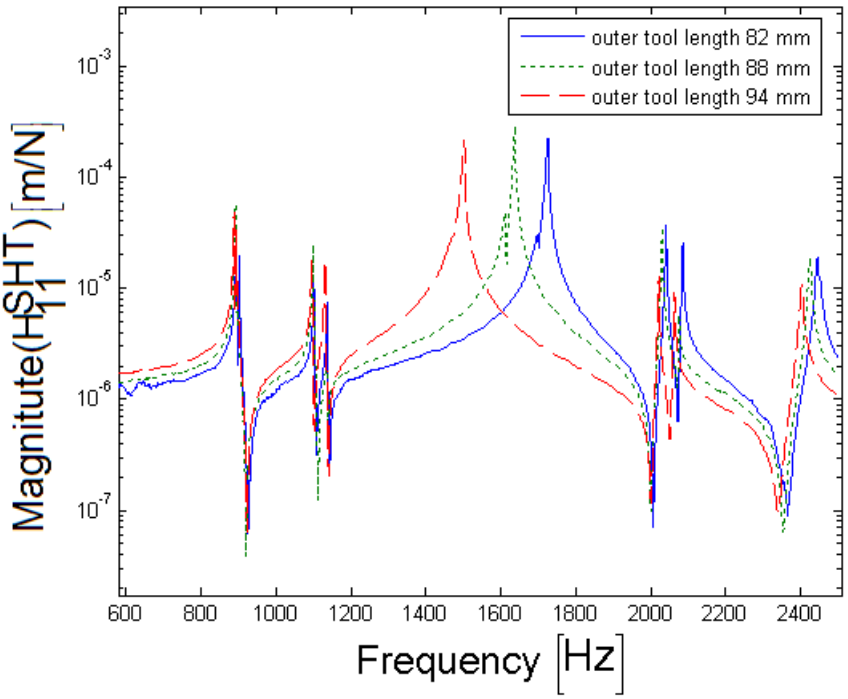

Figure 3.16 Tool point FRF with changing tool length outside the holder.

For a tool overhang length of 49 mm, spindle – holder subassembly, spindle – holder – tool assembly and tool receptance matrices are substituted in Equation 2.3, and the contact parameters are identified. Identified stiffness values are shown in Figure 3.17 – Figure 3.20, whereas the identified damping values are given in Figure 3.21 – Figure 3.24. Note that, the identified contact parameters are not constant in the frequency range, but identification can be done using the results at the tool mode region. These identified values are given in Table 3.1. Also note that, since the L and N FRFs are taken to be identical as given for the spindle-holder subassembly in Figure 3.10 and Figure 3.11 and for the spindle-holder-tool assembly in Figure 3.13 and Figure 3.14 for convenience (with the assumption of reciprocity), 6 distinct values have been identified.

As seen from Figures 3.17 - Figure 3.20, unlike the behavior of the identified stiffness in the frequency band, stiffness values display a convergence behavior in the tool mode region. Therefore the average values of the stiffness values in the tool mode region are taken as identified parameters.

The identified damping values become maximum in the tool mode region and drop to negative values with a sharp decrease as can be seen from Figures 3.21 –Figure 3.24. In the identification procedure these peak values are taken as identified damping values. Accuracy of these identified parameters is checked as shown in Figures 3.25 and Figure 3.26.

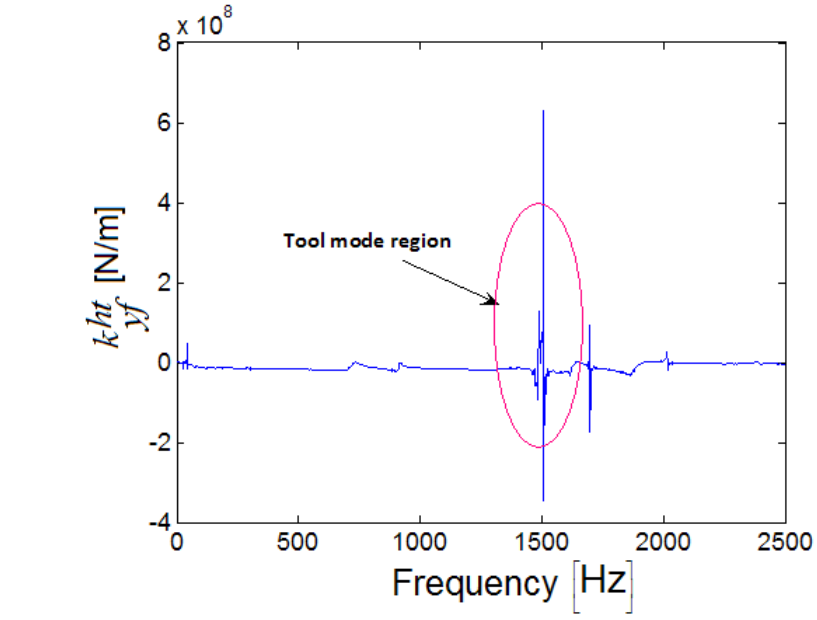

(a)

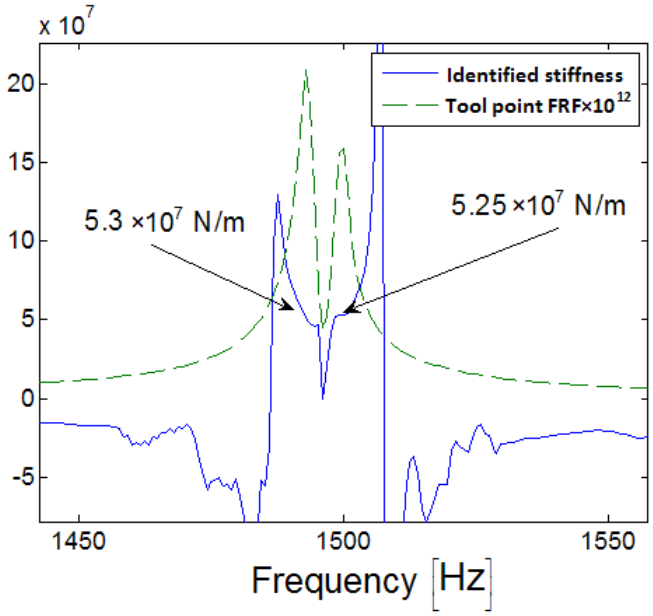

(b)

Figure 3.17(a) Identified linear displacement to force stiffness values (b) Identified linear displacement to force stiffness and tool point FRF at the tool mode region.

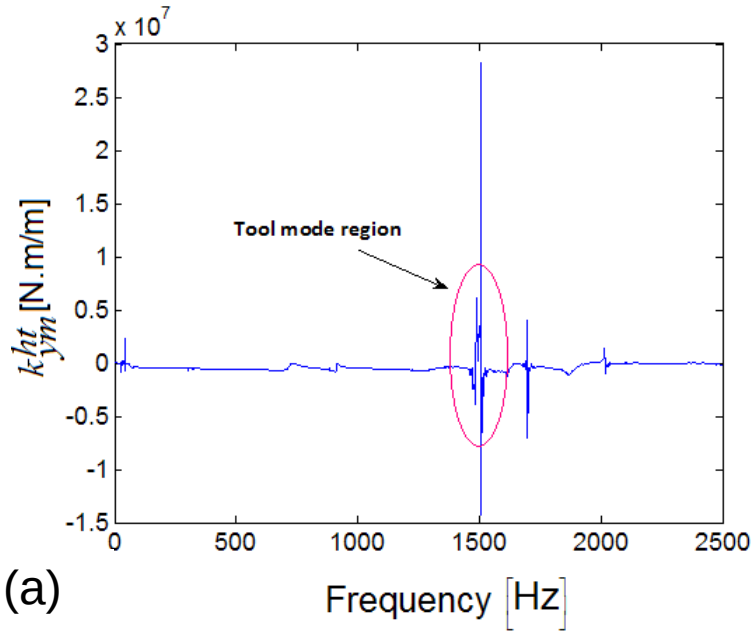

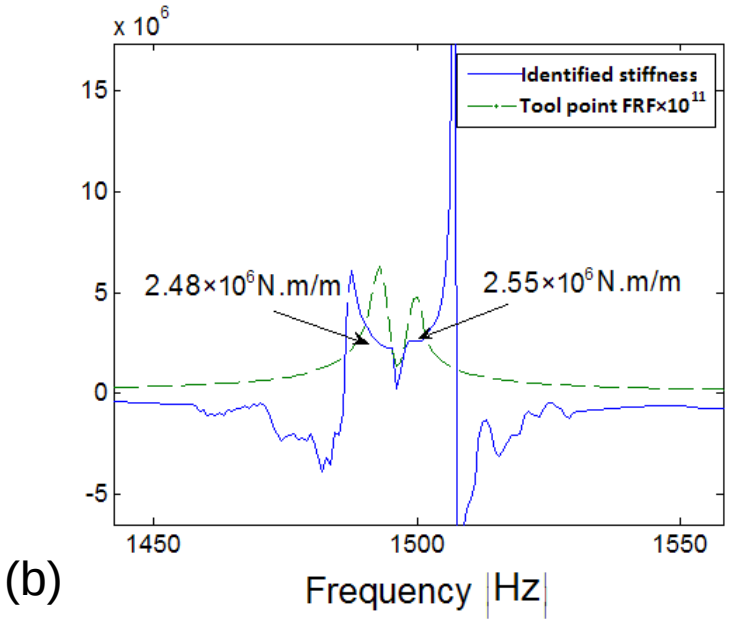

Figure 3.18 (a) Identified linear displacement to moment stiffness values (b) Identified linear displacement to moment stiffness and tool point FRF at the tool mode region.

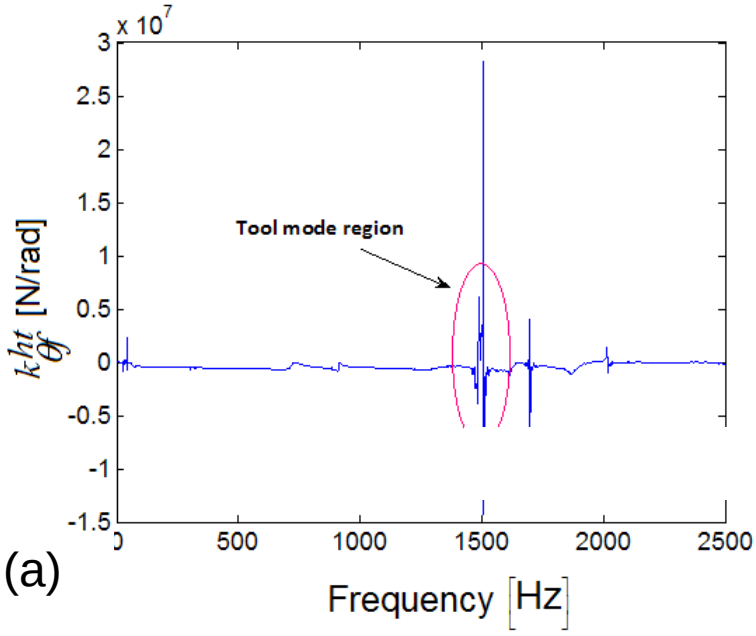

(a)

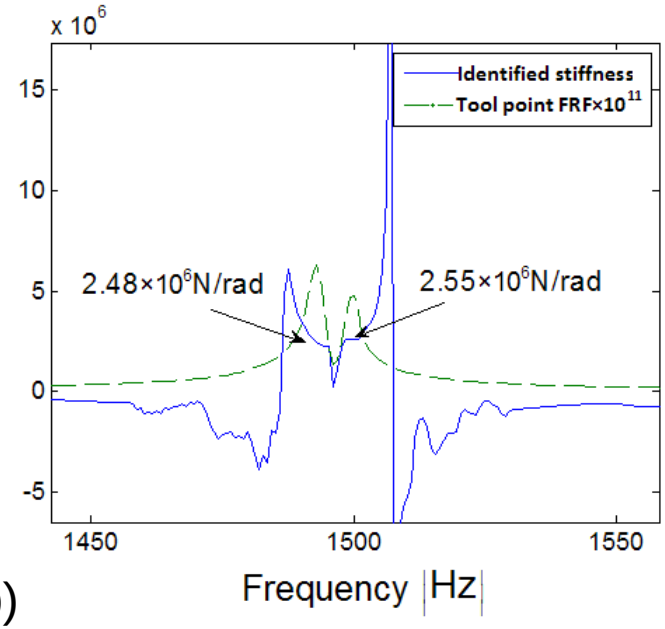

(b)

Figure 3.19 (a) Identified angular displacement to force stiffness values (b) Identified angular displacement to force stiffness and tool point FRF at the tool mode region.

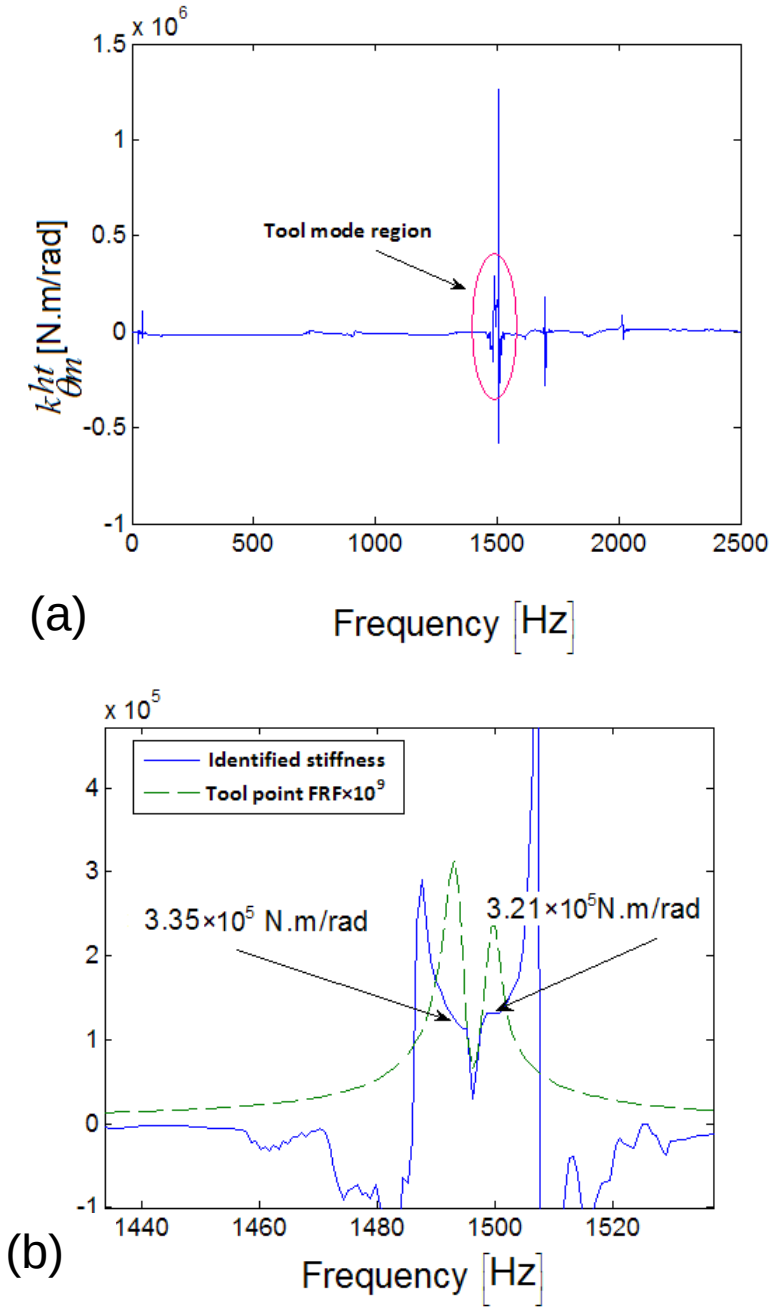

Figure 3.20 (a) Identified angular displacement to moment stiffness values (b) Identified angular displacement to moment stiffness and tool point FRF at the tool mode region.

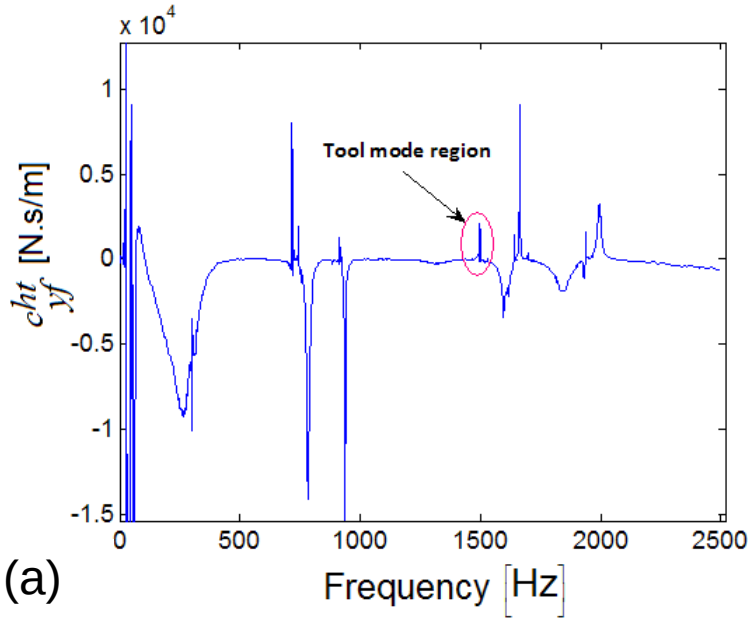

(a)

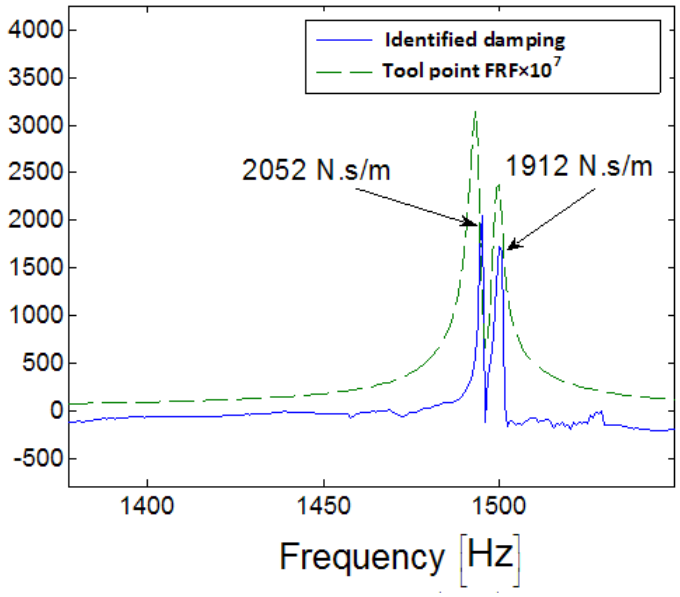

(b)

Figure 3.21 (a) Identified linear displacement to force damping values (b) Identified linear displacement to force damping and tool point FRF at the tool mode region.

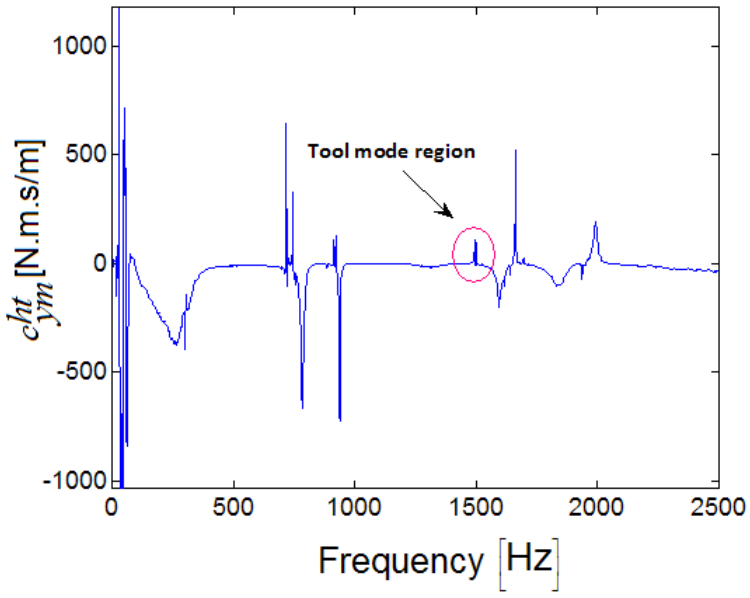

(a)

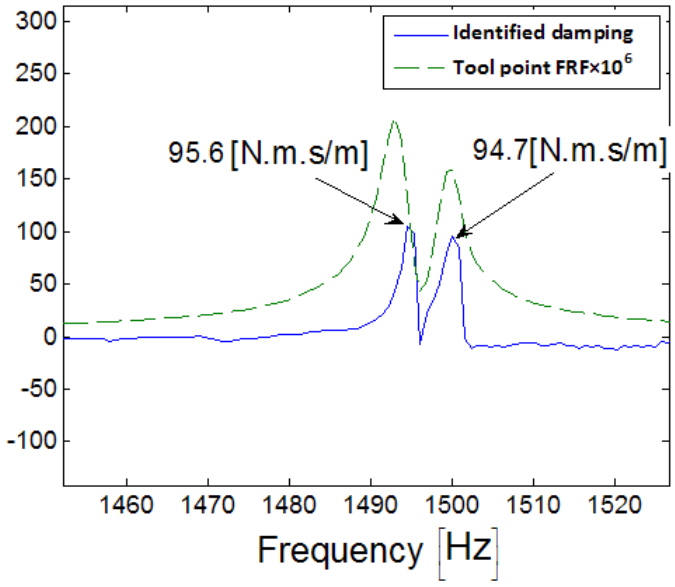

(b)

Figure 3.22 (a) Identified linear displacement to moment damping values (b) Identified linear displacement to moment damping and tool point FRF at the tool mode region.

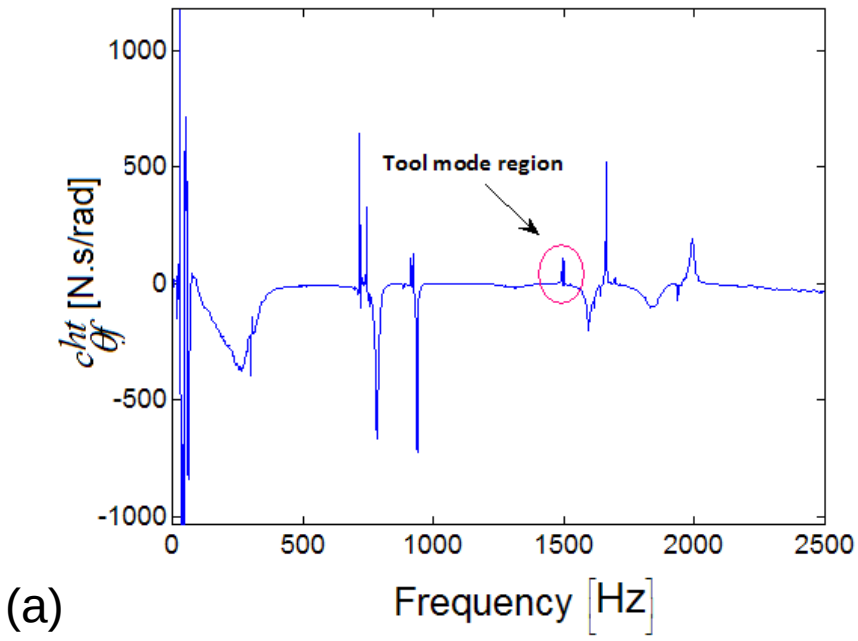

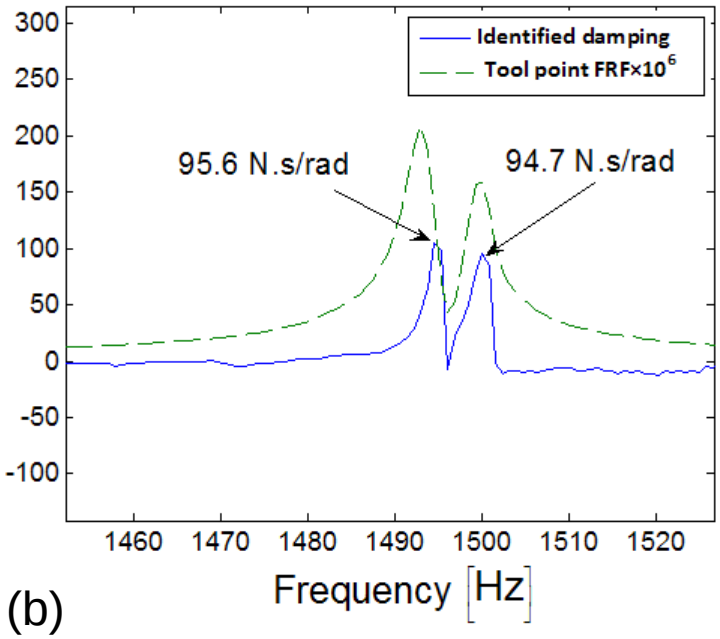

Figure 3.23 (a) Identified angular displacement to force damping values (b) Identified angular displacement to force damping and tool point FRF at the tool mode region

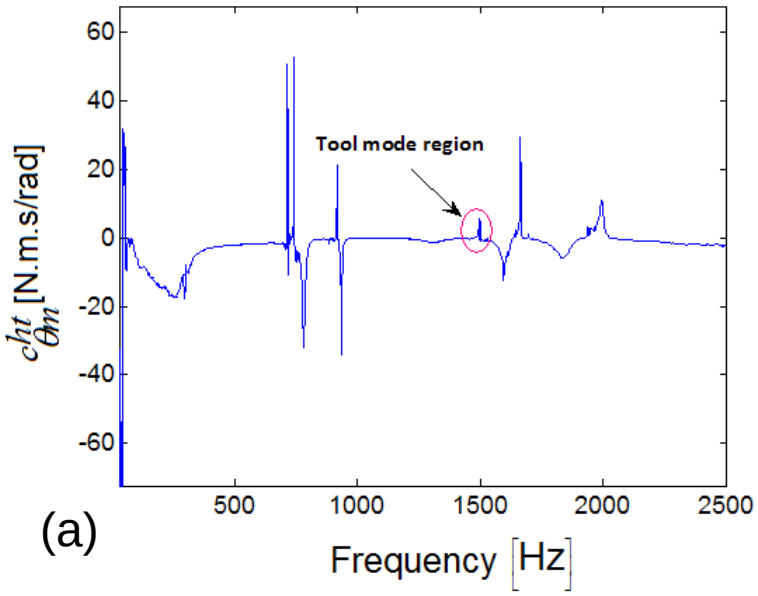

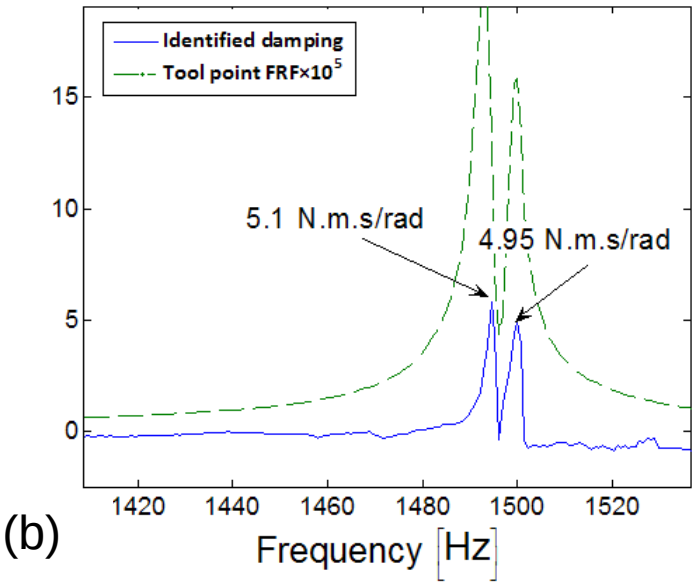

Figure 3.24 (a) Identified angular displacement to moment damping values (b) Identified angular displacement to moment damping and tool point FRF at the tool mode region.

As seen from Table 3.1, in the tool mode region, due to two separate peak values the contact parameters converge to different values but these identified parameters differ from each other with only a small amount. This difference between two peak values is the result of the sensitivity of the method to the experimental inaccuracies due to the matrix inversions.

In order to show the accuracy of the identification method, the experimentally obtained spindle-holder subassembly receptance matrix $\left[SH_{11}\right]$ is coupled with the analytically obtained tool FRFs through the forward coupling equation, Equation (2.3). In the coupling of the spindle-holder and tool subsystems, instead of using frequency dependent contact parameters, the constant values identified from the respective dominant modes of the holder-tool interface (Table 3.1) are used. Also, in order to investigate the effect of the deviation of the contact parameters between two peak values, coupling of the receptance matrices are performed with the identified parameters from both peak values in the tool mode region. Results are shown in Figure 3.25 and Figure 3.26.

Table 3.1 Identified dynamical contact parameters at the holder-tool interface in the experimental case study

	First peak of the tool mode	Second peak of the tool mode
Linear displacement – to – force stiffness (N/m)	5.3×10^{7}	5.2×10^{7}
Linear displacement – to – force damping (N.s/m)	2000	1900
Linear displacement – to - moment stiffness (N.m/m)	2.5×10^{6}	2.6×10^{6}
Linear displacement – to – moment damping (N.m.s/m)	96	95
Angular displacement – to – force stiffness (N/rad)	2.5×10^{6}	2.6×10^{6}
Angular displacement – to – force damping (N.s/rad)	96	95
Angular displacement – to – moment stiffness (N.m/rad)	3.4×10^{5}	3.2×10^{5}
Angular displacement – to – moment damping (N.m.s/rad)	5.1	4.9

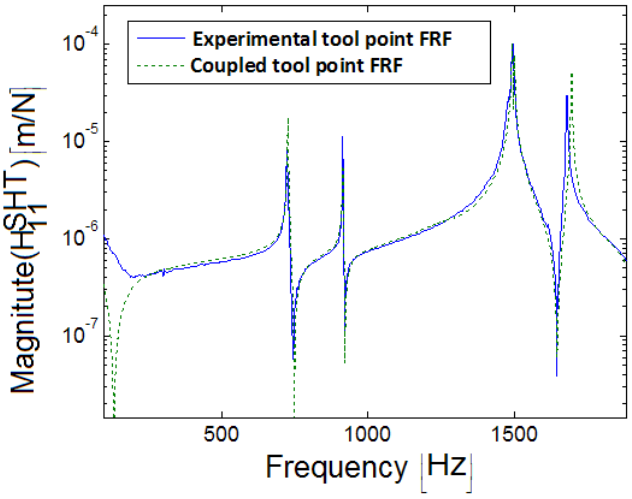

Figure 3.25 Experimentally obtained tool point FRF and the tool point FRF obtained by receptance coupling with the identified contact parameters from the first peak of the tool mode.

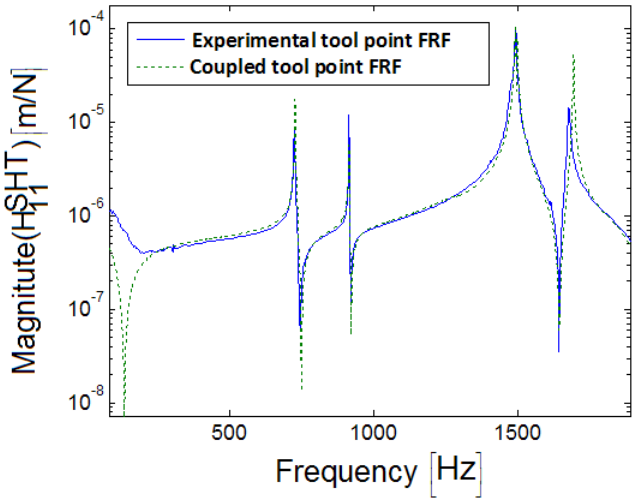

Figure 3.26. Experimentally obtained tool point FRF and the tool point FRF obtained by receptance coupling with the identified contact parameters from the second peak of the tool mode.

As seen from Figures 3.25 and Figure 3.26, small changes in the identified parameters have negligible effect on tool point FRF. Thus, using the identified parameters from the developed method, tool point FRFs can be obtained with a high accuracy.

In this chapter, experimental verification of the method developed is performed. Since the polluted case study given in section 2.3 shows that the method is highly sensitive to the noise in the data, experimental data is filtered with Savitzky Golay filter. Also RDOF related FRFs, which are difficult to measure with experiments, are obtained with finite difference method. Finally, contact parameters are identified form the experimental data. As given in Figure 3.25 and Figure 3.26, the results show that the contact parameters can be identified accurately by using the method developed.

Chapter 4

IDENTIFICATION OF CONTACT PARAMETERS WITH NEURAL NETWORK

4.1 Introduction

Although important progress has been achieved for the identification of contact parameters in spindle-holder-tool assemblies, there is still need for experimentation. Due to the complexity of the contact mechanism, it is difficult to model the contact parameters analytically. In such cases, where the system characteristics are unknown or difficult to identify, artificial neural networks (ANN) provide an efficient tool to predict the system characteristics. Especially in the last two decades, ANN has become an important tool in many engineering applications. ANN learns the system characteristics with limited sets of data pairs, containing inputs and corresponding outputs of the system. This training principle is based on minimization of the error of the neural network for known input – output pairs [26, 27]. Once the network learns the system characteristics, it can provide reasonable results to the inputs. Therefore, a well-trained neural network can be an efficient solution to the identification of contact parameters in developing machining stability diagrams. They can save substantial amount of time and eliminate the need for high number of tests.

4.2 Neural Network Theory

A sample ANN is shown in Figure 4.1 consisting of 3 layers which are input layer, hidden layer and output layer. Each layer contains neurons, weights and activation functions.

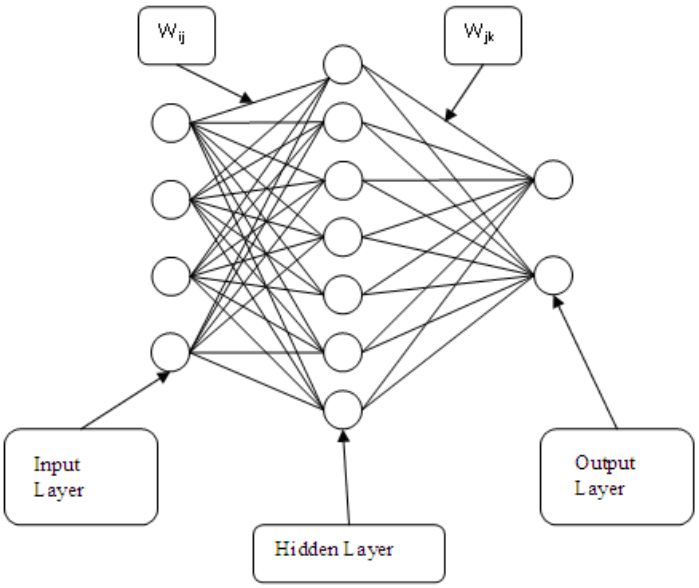

Figure 4.1 Sample neural network and its components.

In neural network connections between input layer and hidden layer are done with w_{ij} weight and connection between hidden layer and output layer is done with w_{jk} weight. , w_{ij} is the connection between i^{th} neuron of input layer and j^{th} neuron of hidden layer, and w_{jk} is the connection between j^{th} neuron of hidden layer and k^{th} neuron of output layer. ANN also contains activation functions. The sum of the

weighted inputs is the input for the activation functions. If the input to the neural network is I input for the j[th] neuron of the hidden layer is given as follows.

$$I_j^{hidden} = \sum_{i=1}^{n} I_j w_{ij} \tag{4.1}$$

An ANN is based on the minimization of the error between expected outputs of the system and the actual output of the neural network. In the ANN the total error is given by the following equation where T is the expected output and O is the actual output:

$$E = \frac{1}{2} \sum_{k=1}^{m} (T_k - O_k)^2 \tag{4.2}$$

In order to minimize the error, weights are updated after each minimization, and the process is finished after the error decreases below the desired value. New values of the weights are given as follows,

$$(w_{ij})_{new} = (w_{ij})_{old} - \Delta w_{ij} \tag{4.3}$$

$$(w_{jk})_{new} = (w_{jk})_{old} - \Delta w_{jk} \tag{4.4}$$

$$\Delta w_{ij} = -\eta \frac{\partial E^2}{\partial w_{ij}} \tag{4.5}$$

$$\Delta w_{jk} = -\eta \frac{\partial E^2}{\partial w_{jk}} \tag{4.6}$$

In Equations (4.5) and (4.6), η is the learning rate used for the arrangement of the convergence rate. When the derivatives in Equations (4.5) and (4.6) are calculated, updated weights w_{jk} and w_{ij} are obtained as follows,

$$(w_{jk})new = (w_{jk})_{old} - \eta(T_k - O_k) f'(I_k) O_j \tag{4.7}$$

$$(w_{ij})new = (w_{ij})_{old} - \eta_i \frac{\partial E^2}{\partial I_k} w_{jk} f'(I_j) \tag{4.8}$$

where f is the activation function in the hidden layer.

A well-trained ANN is highly probable to identify the system characteristics and give reasonable results to inputs which are given to itself for the first time. The most common problem in training neural network is the over fitting of the system which leads to a problem where the system memorizes the training set rather than learning the system characteristics. In order to prevent the over fitting the training set, one method in the literature, is to divide the training set into sub groups and while using one group in training procedure of the ANN, the remaining part of the data set is not given to ANN. After each optimization, error of the ANN to the first seen inputs is checked. When the error of the ANN to the first seen inputs starts to increase, training is stopped. Because in over fitting case, although ANN predicts the output of the data set given in training procedure accurately, they start to give wrong results to the first seen inputs and error to the first seen inputs starts to increase.

4.3 Identification of Contact Parameters

In order to identify the contact parameters at the holder – tool interface, the analytical model proposed by Ertürk et al. [13] is used. The individual receptance matrices of the subassemblies, spindle (*S*), holder (*H*) and tool (*T*) are obtained by rigid coupling of free-free Timoshenko beams. After obtaining receptance matrices of the subassemblies, spindle and holder are coupled through the complex stiffness matrix of the spindle-holder interfaces which is represented by the complex

stiffness matrix $[K_{sh}]$, and thus the spindle – holder subassembly receptance matrix is obtained as follows,

$$[SH_{11}] = [H_{11}] - [H_{12}]\left[[H_{22}] + [K_{sh}]^{-1} + [S_{11}]\right]^{-1}[H_{21}] \tag{4.9}$$

Similarly, the spindle – holder subassembly receptance matrix is coupled with tool receptances through the complex stiffness matrix of the holder tool interface $[K_{ht}]$, and tool point FRF of the spindle – holder – tool assembly is obtained as follows,

$$[SHT_{11}] = [T_{11}] - [T_{12}]\left[[T_{22}] + [K_{ht}]^{-1} + [SH_{11}]\right]^{-1}[T_{21}] \tag{4.10}$$

Spindle – holder and holder – tool interface complex stiffness matrices are respectively given as follows.

$$[K_{sh}] = \begin{bmatrix} k_{yf}^{sh} + i\omega c_{yf}^{sh} & 0 \\ 0 & k_{\theta m}^{sh} + i\omega c_{\theta m}^{sh} \end{bmatrix} \tag{4.11}$$

$$[K_{sht}] = \begin{bmatrix} k_{yf}^{sht} + i\omega c_{yf}^{sht} & 0 \\ 0 & k_{\theta m}^{sht} + i\omega c_{\theta m}^{sht} \end{bmatrix} \tag{4.12}$$

where k_{yf}^{ht} is the linear displacement – to – force stiffness, c_{yf}^{ht} is the linear displacement – to – force damping, , $k_{\theta m}^{ht}$ is the angular displacement – to – moment stiffness and $c_{\theta m}^{ht}$ is the angular displacement – to – moment damping of

the holder-tool interface, ω is the excitation frequency and i is the unit imaginary number.

For simplicity, off diagonal terms of the complex stiffness matrices are taken zero. In order to identify the contact parameters at the holder – tool interface, first spindle, holder and tool subassemblies are obtained analytically. and Then, they are coupled through complex stiffness matrices at the spindle – holder and holder – tool interface, and finally the tool point FRF is obtained analytically. After obtaining it analytically, the tool point FRF is also measured for the same spindle – holder – tool combination. Finally, spindle – holder and holder – tool contact parameters are identified from the relevant frequency regions of interest with the results of effect analysis given by Ertürk et al [17]. According to effect analysis results, contact parameters at the spindle – holder interface mainly affect the first elastic mode and contact parameters at the holder – tool interface affect the second elastic mode. In addition, these modes are mainly affected by the translational parameters as the rotational parameters have negligible effects. Therefore, average values can be used for the rotational parameters in the predictions.

In the experimental set up, BT 40 type holder is assembled to the free spindle where the tool is clamped to the holder via collets. Details of the experimental setup are already given in section 3.1. In order to obtain set of contact parameters to train the ANN, experiments were performed using end mills with different diameters and gauge lengths. Four different tool diameters were used in the tests: 10 mm, 12 mm with, 16 and 20 mm with varying tool gauge lengths. Complete spindle – holder – tool assembly where 12 mm diameter tool is clamped to the holder is shown in Figure 3.4.

As seen the experimental results given in section 3, in the frequency range of interest, the assembly has five distinct peak values. In order to identify the contact

parameters precisely, the tool point FRF was measured for overhang lengths of 74 mm, 80 mm and 86.5 mm for the same tool diameter. Results are shown in Figure 4.2. It is obvious that the only change occurs in the third mode and it can be concluded that the identification of contact parameters at the holder – tool interface can be done from this mode since the tool mode is mainly affected by these contact parameters. Similar, measurements were done for the other tools with different diameters with changing tool length outside the holder.

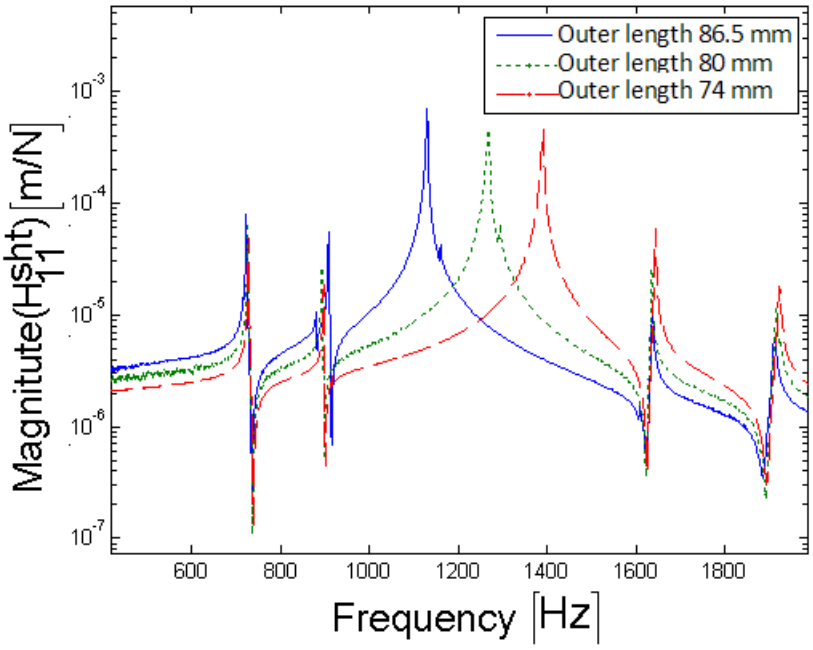

Figure 4.2 Tool point FRFs of the spindle – holder – tool assembly with varying tool length outside the holder.

In addition to the spindle, holder and tool geometries, another possible parameter that might affect the contact parameters and thus the tool point FRF is the clamping torque. In order to see the effect of clamping torque, for the same spindle – holder – tool combination, the tool point FRF was measured for different clamping torques. The tool point FRFs with 20 N.m, 30 N.m and 40 N.m clamping torques for the 12 mm diameter end mill with 76 mm gauge length are shown in Figure 4.3.

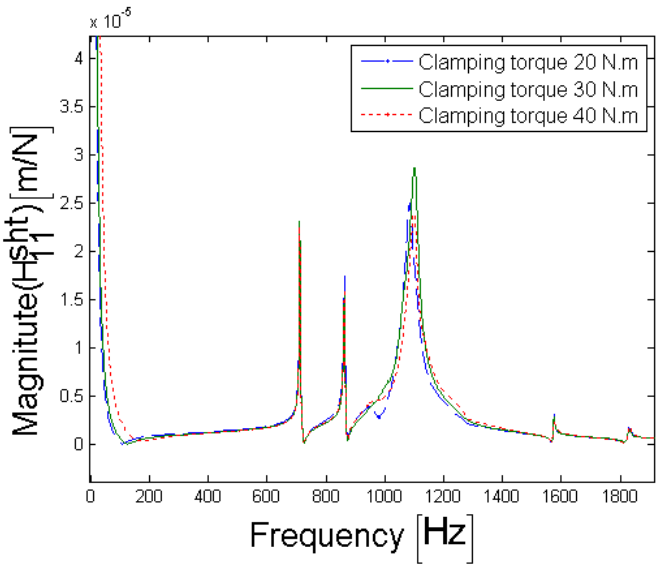

Figure 4.3 Tool point FRF with changing clamping torque.

As it can be seen from Figure 4.3, the clamping torque has a negligible effect on tool point FRF. Therefore, clamping torque of the tool can be neglected, and just the geometry of the tool can be selected as the input to the ANN.

Tool point FRFs were measured for different tool diameter and gauge length combinations, and the contact parameters at the holder – tool interface are identified from the third mode. Identified parameters for the tool with 12 mm diameter and 83 mm gauge length are given in Table 4.1.

Table 4.1 Dynamical contact parameters at the holder-tool interfaces identified for 12 mm diameter tool with 83 mm gauge length.

	Linear displacement to force stiffness (N/m)	Linear displacement to force damping (N.s/m)	Angular displacement to moment stiffness (N.m/rad)	Angular displacement to moment damping (N.m.s/rad)
Spindle – holder interface	4.1×10^7	400	3.5×10^6	7
Holder – tool interface	0.47×10^7	12	8×10^4	4

In order to check the accuracy of the identified contact parameters, the spindle, holder and tool analytical models were coupled through identified contact parameters, and the results are shown in Figure 4.4.

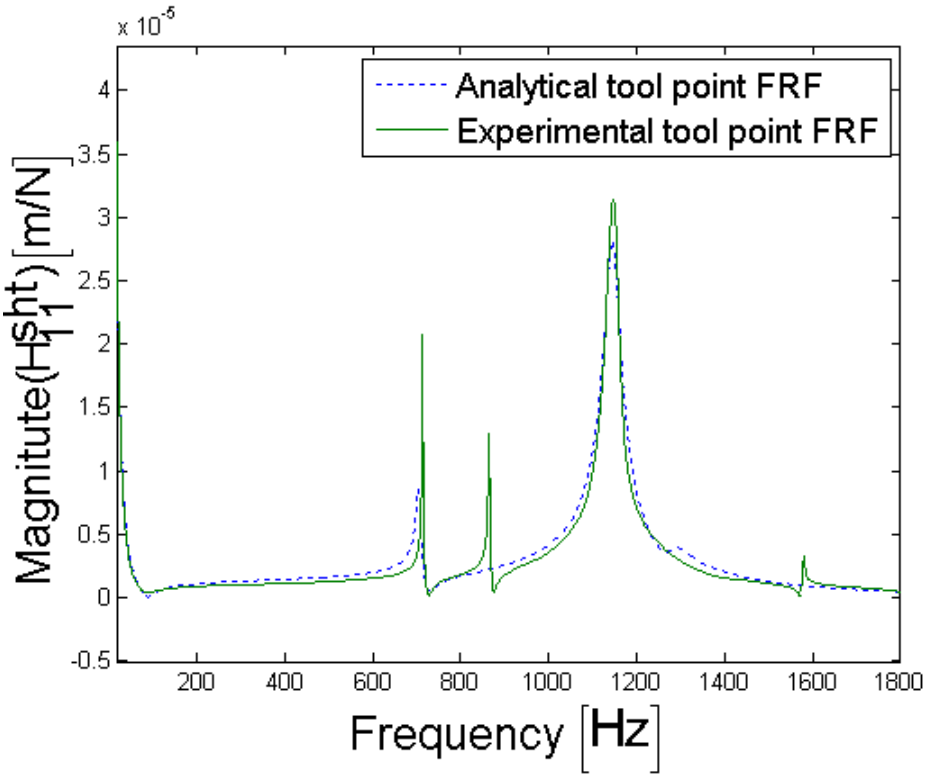

Figure 4.4 Experimentally and analytically obtained (using the identified contact parameters) tool point FRFs for 12 mm diameter tool with 83 mm gauge length.

After obtaining tool point FRF, for given cutting conditions and work material, stability diagrams can be generated using the experimental and analytical FRFs. An example case is shown in Figure 4.5. Stability diagrams are calculated with the software called MADSIM developed during TÜBİTAK supported project under number 104M430.

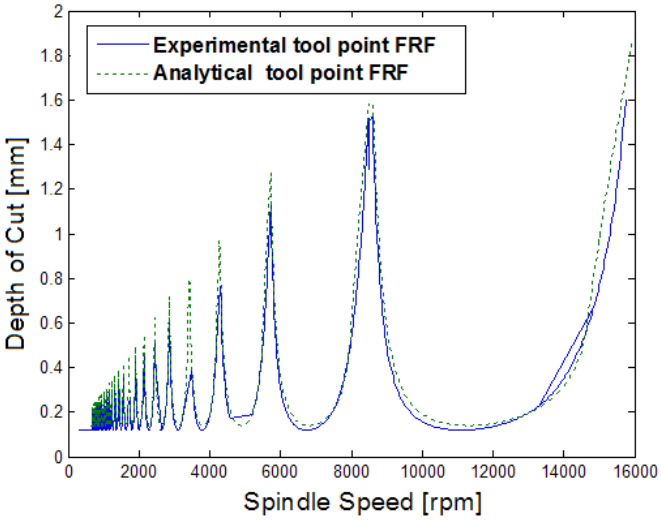

Figure 4.5 Stability lobe diagrams obtained by using experimentally and analytically obtained tool point FRFs for 12 mm diameter tool with 83 mm gauge length.

As can be seen from Figure 4.5, the stability diagram obtained with analytically tool point FRF has very close agreement with the stability diagram obtained from the experimental tool point FRF. Therefore, with the accurate prediction of contact parameters, stable regions in the machining process can be identified precisely.

4.4 Sensitivity of the Tool Point FRF to Contact Parameters

After the identification of the contact parameters at the holder – tool interface for different cases, the effect of the contact parameters on the tool point FRF was analyzed in order to show the importance of accurate identification of these parameters. In this section, the effects of contact parameters are investigated by changing just one parameter and keeping the remaining ones constant.

In order to study the effect of the contact parameters, spindle – holder – tool assembly given in Figure 3.5 is used. For the assembly, 12 mm diameter tool is inserted to the holder with 83 mm gauge length. Identified parameters for this case are given in Table 4.1. First, different linear displacement-to-force contact stiffness values are used: 0.27×10^7 N/m, 0.47×10^7 N/m and 0.97×10^7 N/m. The spindle – holder subassembly receptance is coupled with the tool receptances, and the tool point FRFs are shown in Figure 4.6 are obtained. As shown in Figure 4.6, the linear displacement-to-force contact stiffness affects the tool point FRF substantially, demonstrating the need for accurate knowledge of these parameters in machine tool dynamics and chatter stability analyses.

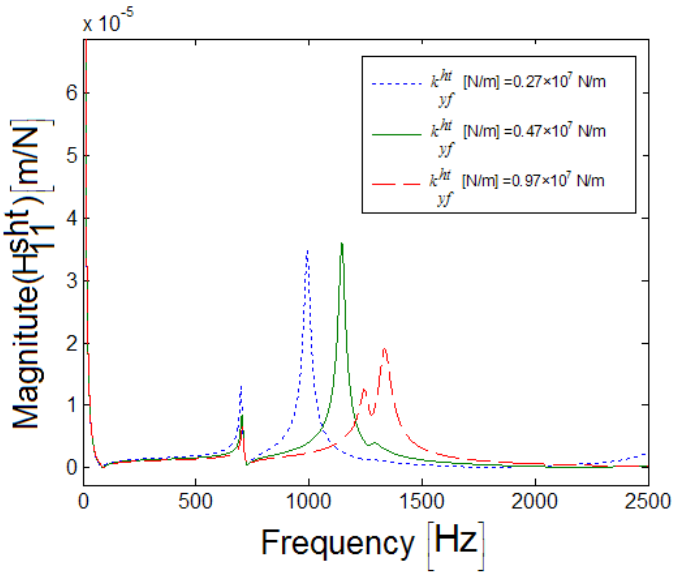

Figure 4.6 Analytically obtained tool point FRFs for different contact translational stiffness.

In order to see the effect of the angular displacement-to-moment stiffness, 6×10^4 N.m/rad, 8×10^4 N.m/rad and12×10^4 N.m/rad were used while keeping the rest of the parameters as given in Table 4.1. The calculated tool point FRFs are given in Figure 12 which indicates that the angular displacement –to-moment contact stiffness does not have a significant effect on the tool point FRF.

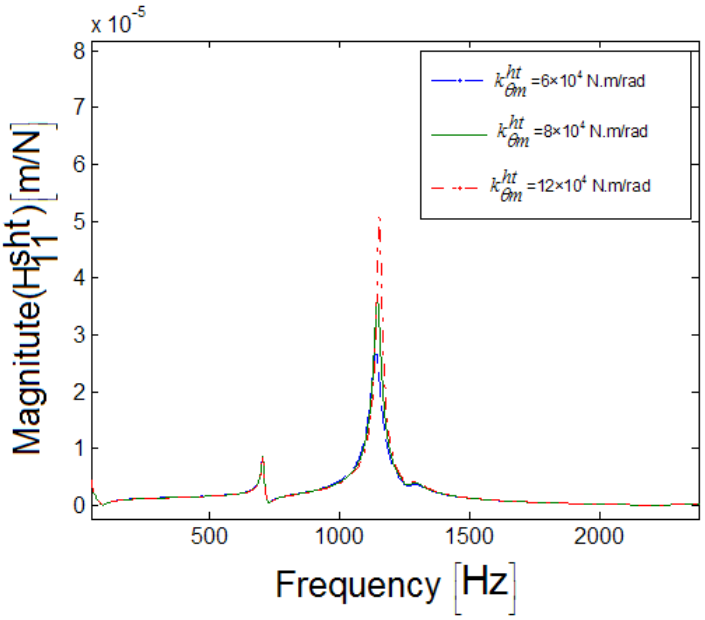

Figure 4.7 Analytically obtained the tool point FRFs using different angular displacement –to-moment contact stiffness.

In addition to the contact stiffness effects on the tool point FRFs, effects of the contact damping were also investigated. With changing values of linear displacement-to-force and angular displacement-to-moment contact damping, the tool point FRFs are given in Figure 13 and Figure 14, respectively. As expected,

the contact damping values affect the magnitude of the tool mode and do not cause tool mode frequency to shift.

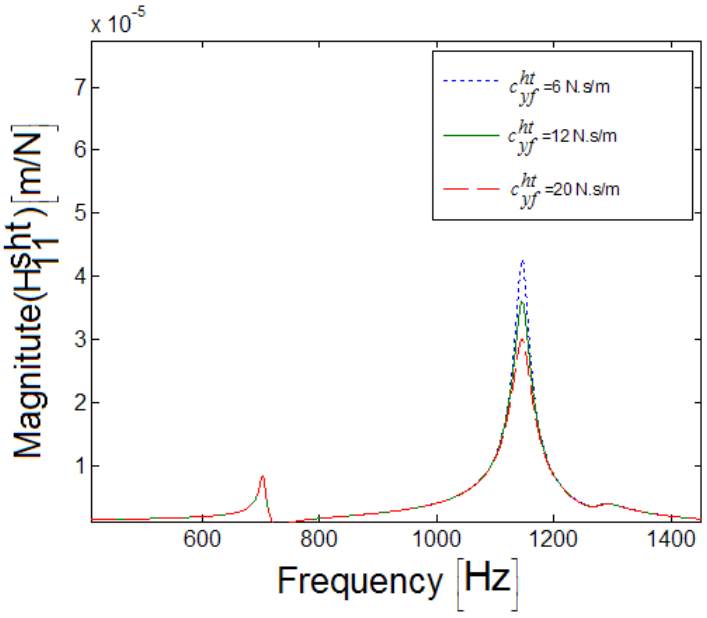

Figure 4.8. Analytically obtained tool point FRFs with different linear displacement-to-force contact damping values.

Results of the sensitivity analysis show that the accurate identification of the contact parameters, especially linear displacement-to-force stiffness plays a crucial role in the accurate determination of the tool point FRF. Therefore in training of ANN variations in rotational damping, rotational stiffness and translational damping values can be neglected for simplicity and as stated by Ertürk et al [16] average values from the literature can be used.

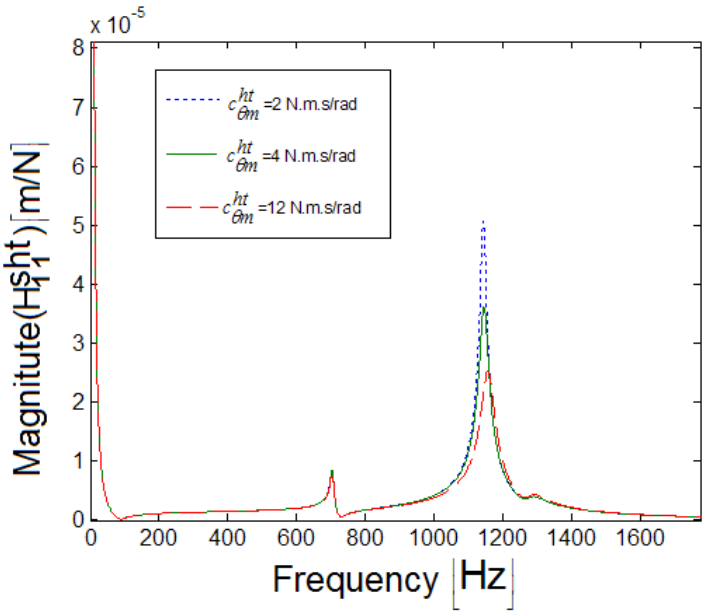

Figure 4.9 Analytically obtained tool point FRFs with different angular displacement-to-moment contact damping values.

4.5 Training of Neural Network and Results

Back propagation ANN was constructed and trained with the identified contact parameters. In ANN, the tool diameter and tool gauge lengths are chosen as inputs, and the linear displacement-to-force stiffness values are set as the output of the ANN. The linear displacement-to-force stiffness is set as output of the ANN since the effect of the rotational parameters is observed to be negligible compared to translational ones. While training the ANN, a limited part of the identified parameters was given to ANN, and the mean square error goal was set to 0.01. When the mean square error reached the desired value, the training was stopped. After the training was completed, the results of the ANN to the inputs used in the

training were checked to confirm that it provided the correct answers. Most important part of the procedure is the ability of the ANN to learn the characteristics of the system rather than memorizing the input – output set. Finally, the inputs that the ANN has never seen were used to predict the outputs, which are given in Table 4.2.

Table 4.2 ANN results for the linear displacement-to-force contact stiffness and the corresponding errors.

Tool diameter (mm)	Gauge length of the tool (mm)	Linear displacement -to-force stiffness (N/m)x10^7	ANN output (N/m)x10^7	Error %
10	65	0.97	0.99	2.10
10	68	0.84	0.87	3.45
10	73	0.58	0.58	0.51
12	76	1.43	1.39	2.80
12	81	1.95	1.98	1.54
12	85	1.20	1.15	4.17
16	83	2.20	2.35	6.82
16	86	2.25	2.22	1.33
16	89	2.20	2.15	2.27
16	92	2.26	2.19	3.10
20	98	3.48	3.49	0.29
20	100	3.68	3.53	4.08
20	106	3.75	3.66	2.40

Results given in Table 4.2 show that the applicability of the ANN in identification of contact parameters is highly effective. The highest error of the neural network to the first seen inputs is less than 7 %.

In order to investigate the effect of using ANN based identified contact parameters in the analytical method, ANN results for the 12 mm diameter tool with 85 mm gauge length were used in the analytical tool point FRF prediction model [13]. The tool point FRFs of the same assembly obtained with the contact parameters identified from experiments are compared with those obtained by using ANN predicted value, which was 4 % different than the experimental value, in Figure 4.10.

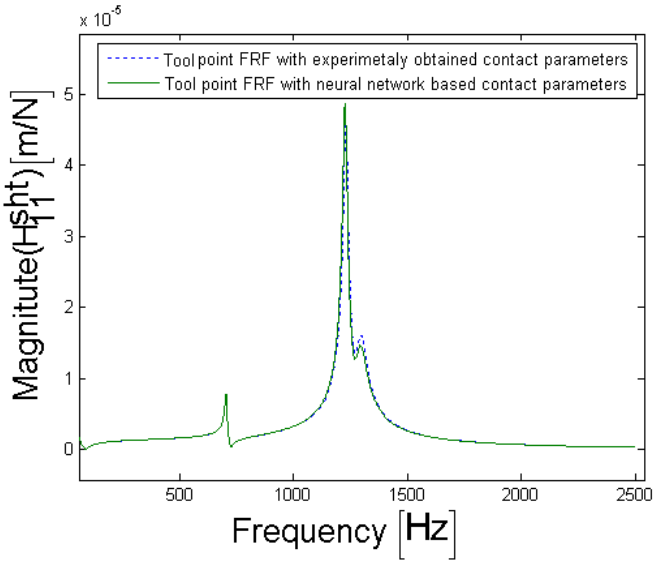

Figure 4.10 Tool point FRF obtained with contact parameters identified with neural network and tool point FRF obtained with contact parameters from experimental results.

As seen from Figure 4.10, 4 % error in the linear displacement-to-force contact stiffness has negligible effect on the tool point FRF. Therefore, it can be concluded that the ANN errors to the first seen inputs are in an acceptable range, and thus ANN predictions can be used in the analytical determination of tool point FRF, and thus in the stability diagrams. Also input parameters to ANN can be increased such that different collet, holder types and different contact mechanisms can be considered in a future work.

Chapter 5

MASS LOADING EFFECT OF ACCELEROMETERS ON TOOL POINT FRF AND STABILITY DIAGRAMS

5.1 Introduction

In tool point FRF measurements, accelerometers are commonly used to obtain the response to impact loading. Although the mass effect of accelerometers is a well known source of measurement errors, due to their simple use, cost benefits and relatively small mass this effect is usually neglected. With the development of the non contact sensors, such as LDV laser vibrometers, the response of the system to a given excitation can be measured more accurately than the accelerometers. However, due to the cost and other practical issues such as the surface conditions of the target point and space limitations, accelerometers are still preferred in many cases. Also, in-process measurements with non contact sensors might be difficult due to the existence of chips and machining processes. In this chapter, experimental errors due to the mass of the accelerometers are investigated. Also, in order to eliminate the mass loading effect of the accelerometers, a structural modification method is presented.

5.2 Experimental Verification of Accelerometer Mass Effect

In order to investigate the mass effect of accelerometers on tool point FRFs, the same spindle – holder – tool assembly tool point FRF was measured using both a 2-gram accelerometer and an LDV laser vibrometer. The test was performed using the experimental setup presented in section 3.2 on a 12 mm diameter tool with 80 mm gauge length. Measured tool point FRF with both measurement device is given in Figure 5.1. As seen from Figure 5.1, the tool point FRF measured with laser vibrometer has a tool mode with peak value at 1444 Hz. However, the tool point FRF measured with accelerometer has the tool mode with peak value at 1277 Hz. This difference can be attributed to the mass of the accelerometer which causes 167 Hz shift of the tool mode. In addition to the accelerometer and laser measurements, in order to verify the fact that the frequency shift of the tool point FRF is mainly due to the additional mass of the accelerometer, the tool point FRF of the spindle-holder-tool assembly with additional mass is measured with laser vibrometer. For the additional mass, accelerometer is attached at the tool tip. Obtained tool point FRF is also given in Figure 5.1. As seen from Figure 5.1, the same amount of frequency shift is observed in additional mass case. Therefore, it can be concluded that the accelerometer measurement causes a significant errors in the tool point FRF which is due to the mass of the measurement device.

The mass of the accelerometer causes a significant shift of the tool mode so that a 15 % error is obtained for the dominant tool mode. Note that the mass effect causes much smaller variation on the frequencies for the other modes of the system as can be seen from the same figure. This is mainly due to the fact that the other modes of the system belong to the spindle and the holder which have much higher mass than the tool. In addition, for these modes the displacement at the tool point where the accelerometer is attached is relatively smaller compared to that of the tool mode.

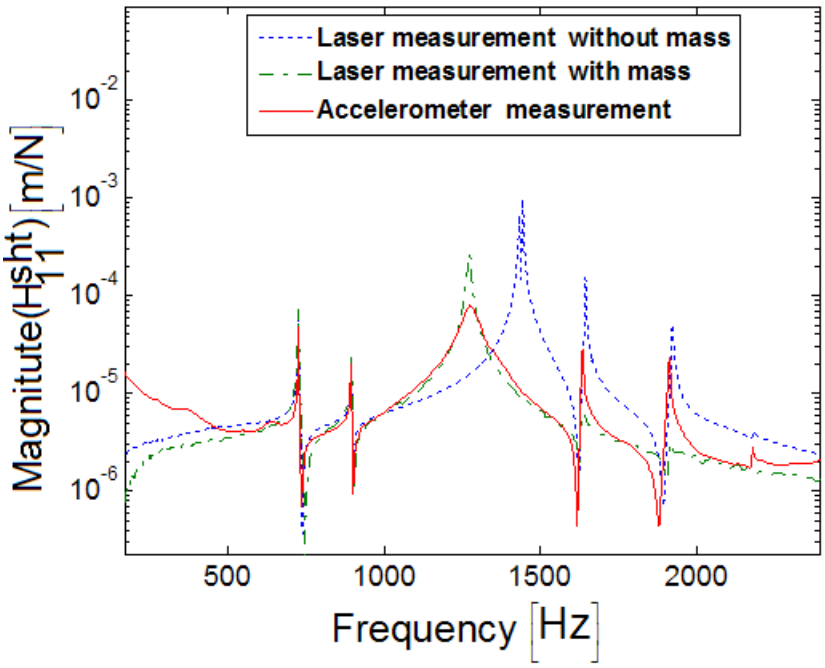

Figure 5.1 Tool point FRF measured with both laser and accelerometer for 12 mm diameter tool with gauge length 80 mm.

In order to identify the effect of the mass of the accelerometer on chatter prediction, stability diagram is calculated for the tool point FRF for the 16 mm diameter tool with 79 mm gauge length for the with and without additional mass cases where the radial depth of cut is 3 mm and number of teeth is 4 for the up milling mode. Also cutting force coefficients are taken as Kt=625 MPa and Kr=100 MPa which represent an aluminum alloy. For the additional mass case frequency shift of the tool mode is 74 Hz. The effect of this error on the stability diagram is given in Figure 5.2, which shows that performing experiments with accelerometer also causes an important deviation in the stability diagram.

Therefore, in a real machining application accelerometer based stability diagrams may make the process completely in the unstable region causing chatter.

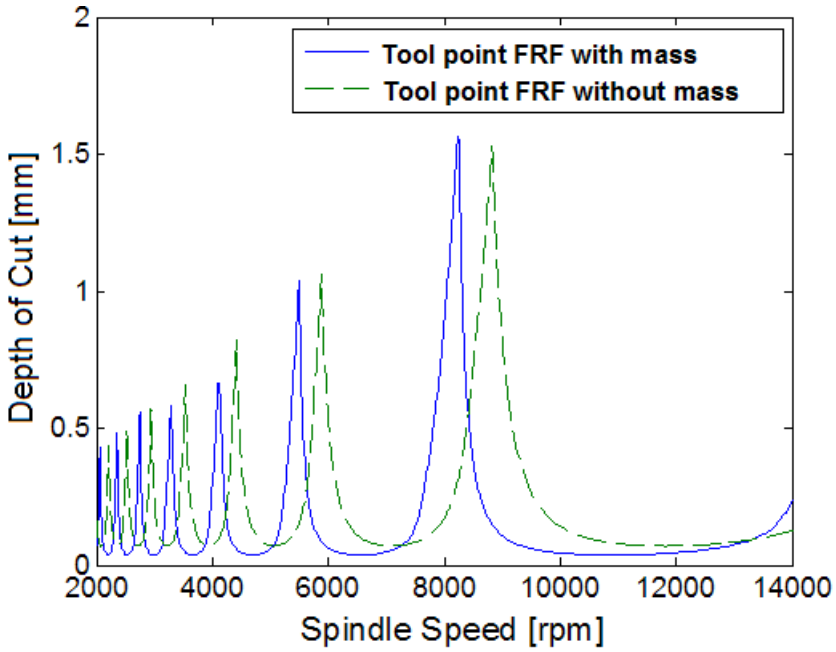

Figure 5.2 Stability diagrams for the tool point FRF with additional mass and without additional mass for the 12 mm diameter tool with 79 mm gauge length.

Frequency shift of the tool mode with respect to tool gauge length is also given in Figure 5.3 for the 16 mm diameter tool. As seen from Table 5.1 and Figure 5.3, with increasing gauge length, the effect of the accelerometer mass is decreasing which is also the case for the increasing tool diameter. This is expected as diameter and length of tools are increased so are their mass. Although the mass effect can be

neglected for large diameter tools, for smaller tools (12 mm diameter and less for the cases considered in this study) the mass effect may cause significant errors in the tool point FRFs, and thus in stability diagrams.

Table 5.1 Frequency change of tool mode peak value due to the mass effect of the accelerometer.

Tool diameter (mm)	Gauge length of the tool (mm)	Tool mode location with laser vibrometer without additional mass (Hz)	Tool mode location with laser vibrometer with additional mass (Hz)	Frequency change (Hz)
10	70	1228	1041	187
10	75	1200	1023	177
12	76	1438	1278	160
12	81	1361	1219	142
12	85	1247	1125	122
16	79	1413	1339	74
16	88	1267	1202	65
16	94	1203	1147	56

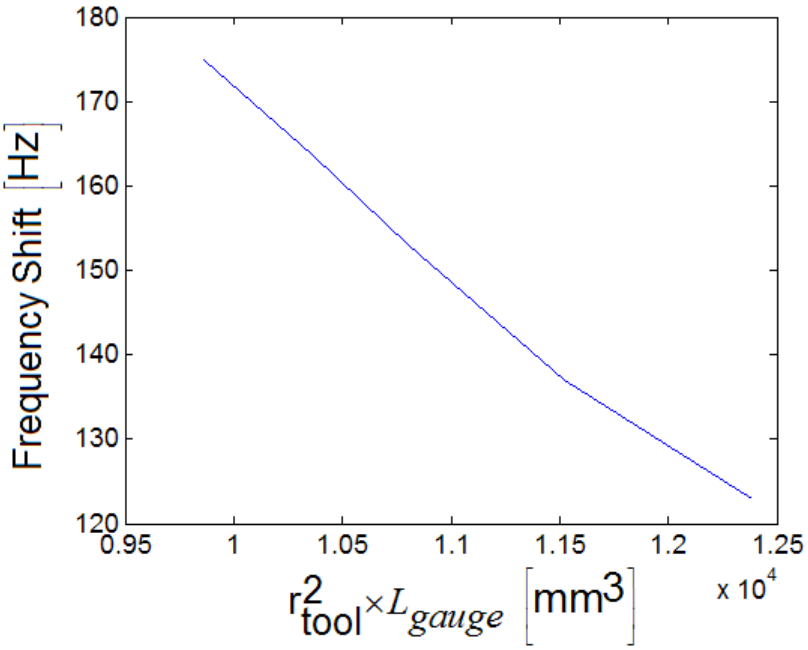

Figure 5.3 Frequency shift of the tool mode with increasing tool gauge length.

5.3 Structural Modification with Matrix Inversion Method

In order to check the accuracy of the experimental results the structural modification method suggested by Özgüven [28] can be applied. In this method, unmodified tool point FRF and mass properties of the modification are used to obtain modified system receptance as follows.

$$\left[SHT_{11}^{modified}\right] = \left[\left[I\right] + \left[SHT_{11}^{unmodified}\right] \times \left[D\right]\right]^{-1} \times \left[\left[SHT_{11}^{unmodified}\right]\right] \tag{5.1}$$

Where, $[I]$ is the identity matrix and $[D]$ is the modification matrix.

Since in accelerometer measurements, the modification on the assembly is only the mass of the accelerometer, and the effect of the mass on the displacement-to-force receptance is being investigated, the modification matrix is a single element given as

$$[D] = (-\omega^2 M) \tag{5.2}$$

and thus Equation (5.1) will take the form,

$$(H_{11}^{sh})_{\mathrm{mod}ified} = (1 + (H_{11}^{sh})_{un\,\mathrm{mod}ified} \times (-\omega^2 M))^{-1} \times (H_{11}^{sh})_{un\,\mathrm{mod}ified} \tag{5.3}$$

Here, M is mass of the accelerometer and ω is the frequency.

Modification method represented by Equation (5.3) is applied to the tool point FRF obtained by the LDV laser vibrometer (for no additional mass case) and the mass modified tool point FRF is obtained. Tool point FRFs measured with and without additional mass are given with the modified tool point FRF in Figure 5.4. As seen from Figure 5.4, with the Matrix Inversion Method, the mass loading effect of the accelerometer can be predicted precisely.

In addition to the application of additional mass in the modification method, the mass effect can also be subtracted from the tool point FRF by using the Matrix Inversion Method as follows,

$$(H_{11}^{sh})_{\mathrm{mod}ified} = (1 + (H_{11}^{sh})_{un\,\mathrm{mod}ified} \times (\omega^2 M))^{-1} \times (H_{11}^{sh})_{un\,\mathrm{mod}ified} \tag{5.4}$$

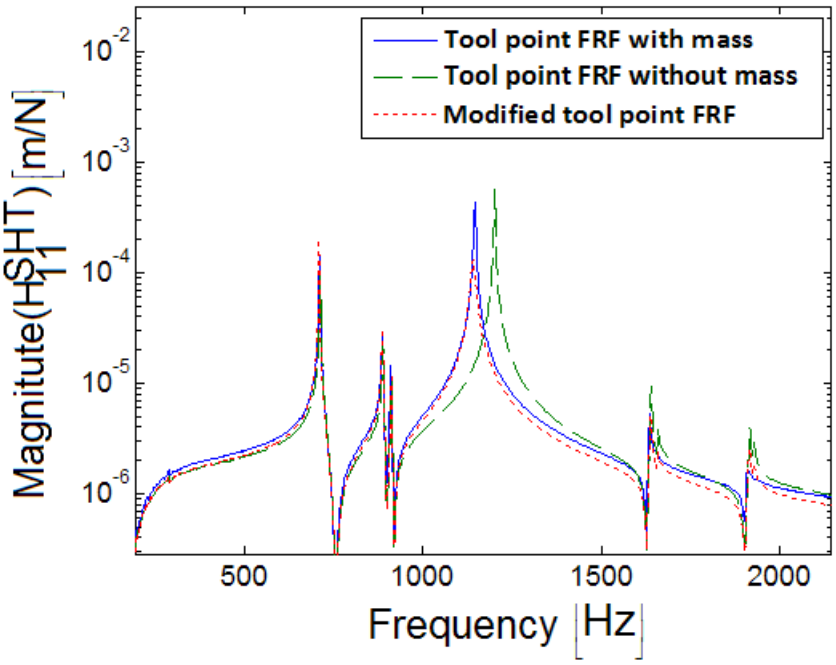

Figure 5.4 Tool point FRF measured with laser vibrometer for with mass, without mass and modified tool point FRF

With Equation (5.4), the mass effect of the accelerometer can be subtracted from tool point FRF. In Figure 5.5, tool point FRF with mass (measured with laser vibrometer), the tool point FRF without mass (measured with laser vibrometer) and the modified tool point FRFs are given. As seen from Figure 5.5, the tool point FRF measured with laser has perfect agreement with the modified tool point FRF. This shows that even when the measurements are performed with an accelerometer, the mass effect can be eliminated by applying the modification.

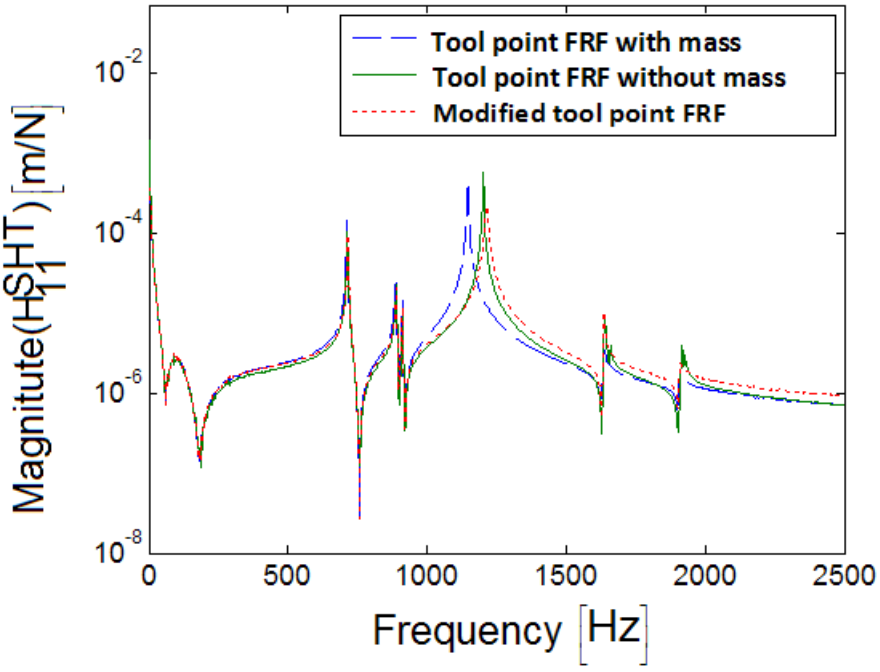

Figure 5.5 Tool point FRF measured with laser vibrometer for with mass, without mass and modified tool point FRF.

In this chapter, a common source of error in measurement of tool point FRF is investigated. Results show that for small diameter tools, performing experiments with accelerometers causes significant errors in the tool point FRF. In order to eliminate the mass effect, a modification method is applied to the accelerometer based tool point FRFs. It is verified with the laser measurements that the mass effect can be compensated satisfactorily by using the modification method.

Chapter 6

CONCLUSION AND SUMMARY

In this thesis, investigation of contact parameters in machining centers is presented. These parameters result from the contacts on the interfacing surfaces of machine tool components, i.e. spindle, holder and tool, and may have significant effects on the dynamic behavior and chatter stability during machining. In order to identify these parameters, the closed form formulation for FRF computation in spindle-holder-tool systems can be rearranged [22]. In this study, the contact parameter identification formulation is improved for obtaining reliable results, and moreover the problems encountered during the practical application of the method in real systems were solved. Thus an effective identification method is developed. The verification of the method suggested is demonstrated with several case studies. Also, as an alternative method, neural network approach is applied for the identification of contact parameters in order to eliminate experimental measurements for each case. The development of methods for accurate identification of contact parameters, and thus tool point FRFs and stability diagrams is the main goal of this thesis.

6.1 A New Approach on Identification of Contact Parameters

First, the details of the experimental method developed are presented. In this method first the receptance coupling equations are rearranged to obtain contact parameters, and a closed form expression is obtained. As an improvement fully

populated complex stiffness matrix is used in the formulation, and to overcome the practical application problems to measure RDOF related FRFs, they are obtained with finite difference method. The method is used for the identification of contact parameters at the holder-tool interface.

First, the method is tested with the analytical case study. It is shown that the method can identify contact parameters accurately. In addition to the success of the method for the analytical case study, the method is tested with the polluted receptance matrices in order to simulate a more realistic scenario. In the polluted case study, it is observed that the proposed method for the identification of contact parameters is highly sensitive to the changes in the receptance matrices. Instead of constant contact parameters, method yields results with frequency depended parameters. Since the identification from the noisy results is impossible, affectivity of the identification of contact parameters from the relevant mode of the tool point FRF is investigated. Although identified contact parameters change with frequency, promising results are obtained from the relevant tool mode. It is also concluded that the sensitivity of the method is mainly due to the matrix inversions in the formulation.

6.2 Experimental Verification of the Proposed Method

It is experimentally verified that the proposed method can identify contact parameters successfully. For the verification of the method, an experimental setup is constructed with real machine parts, and experiments are performed with the laser LDV vibrometer. Since in the method suggested, the receptances of spindle-holder subassembly, spindle-holder-tool assembly and tool are required, both experimental and analytical methods are applied for the determination of these receptance matrices. First, spindle-holder subassembly and spindle-holder-tool assembly displacement-to-force receptances are obtained by performing modal

testing and remaining RDOF related FRFs are obtained with the finite difference method from the experimentally measured receptances. For the determination of tool receptance matrices, Timoshenko beam theory is used and tool receptances are obtained analytically. Before applying experimental data in the method, experimentally obtained data is filtered with the Savitzky Golay filter due to the sensitivity problem of the method, and the identification is performed with the filtered receptances. Although the identification method results contact parameters which vary with frequency and sometimes assume meaningless values, it is observed that these parameters can successfully be identified from the dominant tool mode. Also, the verification of the identified parameters is demonstrated by using these parameters in the receptance coupling equation. The results show that the tool point FRF obtained with the identified contact parameters has a perfect agreement with the experimentally obtained tool point FRF.

6.3 Identification of Contact Parameters with Neural Networks

In order to eliminate the dependency on experiments, as an alternative approach, artificial neural network based identification is presented. For the training procedure of the ANN, contact parameters identified for different tool diameters and gauge lengths are used. It is observed that for the first seen combination of tool diameter and gauge length, ANN can predict corresponding contact parameters successfully. Therefore, by performing experiments with limited sets of spindle- holder-tool combination, contact parameters can be predicted in a wide range of spindle-holder-tool combinations. Elimination of dependency on experiments with the application of the neural network will have an important contribution to the stability diagram studies. This will have advantages in terms of cost and time benefits. Moreover in the design stage of the spindle and holder, it will be possible to predict the stable regions of the designed assembly.

6.4 Mass Loading Effect of the Accelerometers on Tool Point FRF

It is observed that the accurate identification of contact parameters, thus the tool point FRF and stability diagrams, requires reliable experimental data. Since accelerometers are the most commonly used measurement devices in the machine tool dynamics studies, the effect of the accelerometer mass on the tool point FRF is investigated. For that purpose, the tool point FRF is measured both with a laser LDV vibrometer and an accelerometer. From the performed experiments, it is observed that, as the tool diameter decreases, the mass effect of the accelerometer becomes more important and might cause erroneous results. In addition to the error analysis due to the mass of the accelerometer, Özgüven's modification technique is applied in order to eliminate the mass effect. Modification results show that when the measurements are done with an accelerometer, the mass effect can be eliminated and accurate tool point FRFs can be obtained.

6.5 Future Work

Accurate identification of contact parameters plays an important role in accurate tool point FRF determination. Although a closed form approach for the identification of contact parameters is presented in this thesis in detail, there is still a need for the improvement of the method suggested. Most crucial improvement is the sensitivity of the method due to the matrix inversions since a small change in input data may cause large deviations in the output. The possibility of avoiding matrix inversion may be investigated with a modification in the formulation in order to improve the effectiveness of the method. Also, the sensitivity problem may be overcome by applying an alternative method instead of receptance coupling in order to avoid matrix inversions. Another possible improvement is the determination of RDOF related FRFs. With the progress of the measurement

devices, instead of using the finite difference technique, accurate and direct measurement of RDOF related FRF may become available. Therefore with such a technique inaccuracies due to the approximations can be eliminated.

REFERENCES

[1] S.A. Tobias, W. Fishwick, The chatter of lathe tools under orthogonal cutting conditions, Transactions of ASME 80 (1958) 1079-1088.

[2] J. Tlusty, M. Polacek, The stability of machine tools against self-excited vibrations in machining, Proceedings of the ASME International Research in Production Engineering, Pittsburgh, USA, (1963) 465-474.

[3] I. Minis, T. Yanushevsky, R. Tembo, R. Hocken, Analysis of linear and nonlinear chatter in milling, Annals of the CIRP 39 (1990) 459-462.

[4] Y. Altintas, E. Budak, Analytical prediction of stability lobes in milling, Annals of the CIRP 44 (1995) 357-362.

[5] E. Budak, Y. Altintas, Analytical prediction of chatter stability in milling – part I: general formulation; part II: application to common milling systems, Transactions of ASME, Journal of Dynamic Systems, Measurement, and Control 120 (1998) 22-36.

[6] Y. Altintas, Manufacturing Automation, Cambridge University Press, New York, NY, 2000.

[7] T. Schmitz, R. Donaldson, Predicting high-speed machining dynamics by substructure analysis, Annals of the CIRP 49 (1) (2000) 303-308.

[8] T. Schmitz, M. Davies, M. Kennedy, Tool point frequency response prediction for high-speed machining by RCSA, Journal of Manufacturing Science and Engineering 123 (2001) 700-707.

[9] T. Schmitz, M. Davies, K. Medicus, J. Snyder, Improving high-speed machining material removal rates by rapid dynamic analysis, Annals of the CIRP 50 (1) (2001) 263-268.

[10] E.B. Kivanc, E. Budak, Structural modeling of end mills for form error and stability analysis, International Journal of Machine Tools and Manufacture 44 (2004) 1151-1161.

[11] G.S. Duncan, T. Schmitz, An improved RCSA model for tool point frequency response prediction, Proceedings of the 23rd International Modal Analysis Conference, January 30 – February 3, 2005, Orlando, FL (on CD).

[12] A. Ertürk, H.N. Özgüven, E. Budak, Analytical modeling of spindle-tool dynamics on machine tools using Timoshenko beam model and receptance coupling for the prediction of tool point FRF, International Journal of Machine Tools and Manufacture 46 (2006) 1901-1912.

[13] E. Budak, A. Ertürk, H.N. Özgüven, A modeling approach for analysis and improvement of spindle-holder-tool assembly dynamics, Annals of the CIRP 55 (2006) 369-372.

[14] A. Ertürk, E. Budak, H.N. Özgüven, Selection of design and operational parameters in spindle-holder-tool assemblies for maximum chatter stability by using a new analytical model, International Journal of Machine Tools and Manufacture 47 (2007)1401-1409.

[15] T. Schmitz, K. Powell, D. Won, G.S. Duncan, W.G. Sawyer, J.C. Ziegert, Shrink fit tool holder connection stiffness/damping modeling for frequency response prediction in milling, International Journal of Machine Tools and Manufacture 47 (2007) 1368-1380.

[16] K. Ahmadi, H. Ahmadian, Modeling machine tool dynamics using a distributed parameter tool-holder joint interface, International Journal of Machine Tools and Manufacture 47 (2007) 1916-1928.

[17] A. Ertürk, H.N. Özgüven, E. Budak, Effect analysis of bearing and interface dynamics on tool point FRF for chatter stability in machine tools by using a new analytical model for spindle-tool assemblies, International Journal of Machine Tools and Manufacture 47 (2007) 23-32.

[18] E.I. Rivin, Stiffness and Damping in Mechanical Design, Marcel Dekker Press, 1999.

[19] W. Liu, D.J. Ewins, Neural networks: A method for joint dynamic parameter identification, Proceedings of SPIE, the International Society for Optical Engineering, 4359 (2) (2001) 1490-1496.

[20] Y. Kang, C.C. Huang, C.S. Lin, P.C. Shen, Y.P. Chang, Stiffness determination of angular contact ball bearings by using neural networks, Tribology International, 39 (2006) 461-169.

[21] A. Savitzky, M.J.E. Golar, Smoothing and differentiation of data by simplified least squares procedures, Analytical Chemistry 36 (1964) 1627-1639.

[22] O. Özşahin, A. Ertürk, H.N. Özgüven, E. Budak, A Closed-Form Approach for Identification of Dynamical Contact Parameters in Spindle-Holder-Tool Assemblies, International Journal of Machine Tools and Manufacture, 2008, in press.

[23] I.S. Sokolnikoff, Mathematical Theory of Elasticity, McGraw-Hill, New York, 1946.

[24] M. L. M. Duarte, D. J. Ewins, Rotational degrees of freedom for structural coupling analysis via finite-difference technique with residual compensation, Mechanical Systems and Signal Processing 14 (2) (2000) 205-227.

[25] D. J. Ewins, Modal Testing: Theory, Practice and Application, Research Studies Press, 2000.

[26] P. Hajela, L. Berke, Neural network in structural analysis and design, Compput. Struct. 41 (1991) 657-667.

[27] L. Zhang, G. Subbarayan, An evaluation of back propagation neural networks for the optimal design of structural systems. Comput. Methods Appl. Mech. Eng. 191 (2002) 2873-2886.

[28] H. N. Özgüven, Structural Modifications Using Frequency Response Functions, Mechanical Systems and Signal Processing 4 (1990) 53-63.